

Emergence of Recombinant Forms of HIV: Dynamics and Scaling

Gajendra W. Suryavanshi, Narendra M. Dixit*

Department of Chemical Engineering, Indian Institute of Science, Bangalore, India

The ability to accelerate the accumulation of favorable combinations of mutations renders recombination a potent force underlying the emergence of forms of HIV that escape multi-drug therapy and specific host immune responses. We present a mathematical model that describes the dynamics of the emergence of recombinant forms of HIV following infection with diverse viral genomes. Mimicking recent in vitro experiments, we consider target cells simultaneously exposed to two distinct, homozygous viral populations and construct dynamical equations that predict the time evolution of populations of uninfected, singly infected, and doubly infected cells, and homozygous, heterozygous, and recombinant viruses. Model predictions capture several recent experimental observations quantitatively and provide insights into the role of recombination in HIV dynamics. From analyses of data from single-round infection experiments with our description of the probability with which recombination accumulates distinct mutations present on the two genomic strands in a virion, we estimate that ~8 recombinational strand transfer events occur on average (95% confidence interval: 6–10) during reverse transcription of HIV in T cells. Model predictions of virus and cell dynamics describe the time evolution and the relative prevalence of various infected cell subpopulations following the onset of infection observed experimentally. Remarkably, model predictions are in quantitative agreement with the experimental scaling relationship that the percentage of cells infected with recombinant genomes is proportional to the percentage of cells coinfecting with the two genomes employed at the onset of infection. Our model thus presents an accurate description of the influence of recombination on HIV dynamics in vitro. When distinctions between different viral genomes are ignored, our model reduces to the standard model of viral dynamics, which successfully predicts viral load changes in HIV patients undergoing therapy. Our model may thus serve as a useful framework to predict the emergence of multi-drug-resistant forms of HIV in infected individuals.

Citation: Suryavanshi GW, Dixit NM (2007) Emergence of recombinant forms of HIV: Dynamics and scaling. *PLoS Comput Biol* 3(10): e205. doi:10.1371/journal.pcbi.0030205

Introduction

During the reverse transcription of HIV in an infected cell, the viral enzyme reverse transcriptase switches templates frequently from one genomic RNA strand of a virion to the other, yielding a recombinant proviral DNA that is a mosaic of the two parent genomes. If one strand contains a mutation that confers upon HIV resistance to one administered drug and the other strand resistance to another drug, recombination may bring the two mutations together and give rise to progeny genomes resistant to both those drugs [1,2]. Recombination may thus accelerate the emergence of multi-drug resistance in infected individuals. A prerequisite for recombination to induce genomic diversification is the presence of heterozygous virions [3], which contain non-identical genomic RNA strands and are formed when individual cells are infected by multiple virions. Recent experiments present evidence of the predominance of multiple infections of cells both in vitro and in vivo [4–7]: infected splenocytes from two HIV patients, for instance, were found to harbor up to eight proviruses, with three to four proviruses per cell on average [6]. The high incidence of multiple infections of cells coupled with the high recombination rate of HIV, estimated to be several times greater than the HIV point mutation rate [7–10], sets the stage for recombination to act as a powerful agent driving the emergence of multi-drug-resistant forms of HIV in patients undergoing therapy. In addition, recombination may serve to preserve diversity in genomic regions not affected by bottlenecks introduced by drug therapy or host immune responses,

and improve the adaptability of HIV to new environments [11]. Indeed, in addition to several circulating recombinant forms of HIV, a large number of recombinant forms unique to individuals have been identified [12]. It is of great importance, therefore, to understand how recombinant forms of HIV arise in infected individuals.

Remarkable insights into HIV recombination emerge from recent in vitro experiments, in which target cells were simultaneously exposed to two kinds of reporter viruses, and cells infected with recombinant proviruses detected [3–5,7,13,14]. Rhodes et al. determined using single-round infection assays that the likelihood of the accumulation by recombination of distinct mutations present on the two viral genomes in a virion increases with the separation between the mutations and reaches an asymptotic maximum at a separation of ~1,500 base pairs [14]. Further, Rhodes et al.

Editor: Sebastian Bonhoeffer, Swiss Federal Institute of Technology Zurich, Switzerland

Received: May 7, 2007; **Accepted:** September 5, 2007; **Published:** October 26, 2007

A previous version of this article appeared as an Early Online Release on September 6, 2007 (doi:10.1371/journal.pcbi.0030205.eor).

Copyright: © 2007 Suryavanshi and Dixit. This is an open-access article distributed under the terms of the Creative Commons Attribution License, which permits unrestricted use, distribution, and reproduction in any medium, provided the original author and source are credited.

Abbreviations: CFP, cyan fluorescent protein; GFP, green fluorescent protein; YFP, yellow fluorescent protein

* To whom correspondence should be addressed. E-mail: narendra@chemeng.iisc.ernet.in

Author Summary

Retroviral recombination, a process akin to sexual reproduction in higher organisms, may accelerate the accumulation of mutations and the development of multi-drug resistance in HIV patients. Recombination occurs when the enzyme reverse transcriptase switches between the two RNA strands of a virion, yielding a provirus that is a mosaic of the two strands. The latter strands are often distinct, thereby allowing recombinational diversification, when multiple viruses infect individual cells. The enormous HIV recombination rate and recent evidence of frequent multiple infections of cells render recombination a powerful force underlying the development of multi-drug resistance *in vivo*. The dynamics of the emergence of recombinant genomes, however, remains poorly understood. Recent experiments allow a closer look at HIV recombination: cells are exposed to two kinds of reporter viruses and the frequency of recombinant proviruses is detected, which enables direct quantification of the extent of recombination. The observations, however, are not described by available models, leaving a gap in our understanding of HIV recombination. We present a model that describes HIV dynamics with multiple infections of cells and recombination, captures several recent experimental observations quantitatively, provides insights into HIV recombination, and presents a framework for describing the development of multi-drug resistance in HIV patients.

found that the cell type employed for infection—CD4⁺ T cells or macrophages, for instance—does not influence the recombination rate. In contrast, Levy et al. argue that subtle virus–cell interactions cause recombination to occur at different rates in different types of cells [7]. Further, using replication-competent reporter viruses, Levy et al. investigated the dynamics of the emergence of recombinant genomes *in vitro* and in SCID-hu mice [7]. Interestingly, Levy et al. observed two scaling patterns. First, the percentage of cells coinfecting with both the reporter genomes employed for infection was proportional to the total percentage of infected cells. Second, the percentage of cells infected with recombinant proviruses was linearly proportional to the percentage of coinfecting cells and, correspondingly, proportional to the square of the total percentage of infected cells. Further, Levy et al. found that the scaling patterns were independent of the initial viral load, the time following the onset of infection, and whether the experiments were conducted *in vitro* or in SCID-hu mice.

Standard models of viral dynamics, which successfully describe short-term (a few weeks) viral load changes in patients undergoing therapy, are predicated on the infection of individual cells by single virions and ignore recombination [15–17]. Recent modeling advances and simulations incorporate descriptions of multiple infections of cells and recombination, and present insights into the subtle interplay between mutation, recombination, fitness selection, and random genetic drift that underlies the genomic diversification of HIV *in vivo* [18–23]. Bretscher et al. developed a model of HIV dynamics that includes mutation, double infections of cells, and recombination and found that for infinitely large cell populations, the influence of recombination on the development of drug resistance depends sensitively on epistasis, *i.e.*, on the nature of fitness interactions between mutations [20]. Bretscher et al. argue that phenotypic mixing—the assortment of viral proteins arising from different proviral genomes within a multiply infected cell during

the assembly of progeny virions—compromises the selective advantage of the fittest strains and enhances the relative abundance of less fit strains: less fit strains piggyback on fitter strains. At the same time, in a two-locus/two-allele model, recombination, which breaks nonrandom associations of mutations and hence lowers linkage disequilibrium, enhances the relative abundance of single mutant strains compared to wild-type and of double mutant strains when fitness interactions result in positive epistasis, *i.e.*, when mutations interact antagonistically in lowering viral fitness. Bretscher et al. predict, contrary to the prevalent paradigm, that phenotypic mixing and positive epistasis together result in a deceleration of the growth of drug-resistant viruses upon increasing the recombination rate [20]. Recent experimental evidence points to a mean positive epistasis underlying fitness interactions in HIV-1, which, following the predictions of Bretscher et al. [20], raises questions about the benefits of recombination to HIV-1 and, more generally, of the evolutionary origins of recombination and sexual reproduction [24].

Fraser presents a detailed model of HIV dynamics considering up to three infections of cells, mutation, recombination, fitness selection, and different dependencies of the frequency of multiple infections of cells on the viral load [22]. In agreement with Bretscher et al. [20], Fraser found that recombination inhibits the development of drug resistance during antiretroviral therapy and, further, that this effect is modulated not only by epistasis but also by the dependence of the frequency of multiple infections on viral load [22].

In a more recent study, Althaus and Bonhoeffer extend the description of Bretscher et al. [20] to finite population sizes, where the relative abundance of different mutant strains may be determined stochastically rather than deterministically [18]. Interestingly, Althaus and Bonhoeffer found that even when positive epistasis governs fitness interactions between resistance mutations, recombination may significantly accelerate the development of drug resistance when the effective population size is $\sim 10^4$ – 10^5 [18]. Using bit-string simulations, Bocharov et al. found that multiple infections of cells and recombination act in synergy to enhance viral genomic diversity [19], which in turn may increase the likelihood of the emergence of drug resistance. Bocharov et al. note, however, that the time for the selection of fitter genomes that contain multiple mutations may be highly variable, indicative of the stochastic nature of viral evolution *in vivo* [19]. Rouzine and Coffin developed a description of viral evolution with fitness selection, recombination between multiple loci, and random genetic drift, and predict that below a critical population size, the viral population within an individual may converge to a clone in the absence of mutation, leaving little scope for recombination to introduce genomic diversification [23]. Rouzine and Coffin suggest therefore that a reduction of the viral population in an infected individual by combination antiretroviral therapy may decelerate significantly the emergence of drug resistance [23]. The effective population size *in vivo* remains to be established [25].

Currently available models thus make valuable predictions of the influence of recombination on HIV dynamics and the emergence of drug resistance in infected individuals undergoing therapy. The predictions, however, are diverse and have not been compared with available experimental data [3–

5,7,13,14]. An important gap thus exists in our understanding of HIV recombination. Consequently, for instance, the origins of the experimental scaling and dynamical patterns associated with HIV recombination [7] remain poorly understood. Similarly, the recombination rate, or the frequency of template switching events during reverse transcription, remains to be established [7,14].

One limitation of currently available models lies in the approximate descriptions of the dynamics of multiple infections of cells employed. For example, the frequency with which cells are doubly infected is assumed either to be constant [18,20], proportional to the viral load, or proportional to the square of the viral load [22]. Because multiple infections of cells are a prerequisite for the formation of heterozygous virions, an accurate description of HIV dynamics with recombination depends critically on the underlying description of multiple infections, as suggested also by Fraser [22]. The frequency of multiple infections depends not only on the viral load, but also on CD4 down-modulation induced by viral gene expression following the first infection of a cell [26–28], which lowers the susceptibility of the cell to further infections. In a recent study, Dixit and Perelson developed a model that explicitly accounts for CD4 down-modulation and presents a rigorous description of the orchestration of multiple infections of cells by free virions [29]. The model elucidates the origins of one of the two scaling relationships observed by Levy et al. [7]: that the number of doubly infected cells is proportional to the square of the total number of infected cells. Levy et al. note that at the onset of infection in their experiments, because equal numbers of the two kinds of reporter viruses are employed, the probability that a cell is infected with both the reporter genomes is the product of the probabilities that the cell is infected independently with each of the genomes, which explains the origin of the observed scaling early during infection. Later in the infection process, multiple infections of a cell need not be simultaneous and may be sequential. Yet, the quadratic scaling persists. Levy et al. speculate that the absence of any functional hindrance to multiple infections may underlie the persistence of the scaling throughout the infection period. The inhibition of multiple infections by CD4 down-modulation, however, may not be negligible. Dixit and Perelson consider the expected inhibition of multiple infections by CD4 down-modulation and identify conditions under which the observed scaling relationship may hold [29].

The latter model, however, does not distinguish between different viral genomes that infect cells and thereby precludes a description of recombination. Thus, for instance, the dynamics of the emergence of recombinant genomes and the origins of the second scaling relationship observed by Levy et al.—that the percentage of cells infected by recombinant genomes is linearly proportional to the percentage of cells coinfecting with both the reporter genomes employed for infection—remain to be elucidated.

The analysis of Dixit and Perelson [29] provides insights into the origins of the latter scaling. According to the analysis, one set of conditions under which the quadratic scaling between the population of coinfecting cells and that of all infected cells holds occurs at time periods that are long compared to the characteristic viral production and clearance times, so that viral populations are in pseudo equilibrium with the infected cell populations [29]. Under the same

conditions, when two distinct reporter genomes are employed for infection, the population of heterozygous virions containing a copy each of the two reporter genomes is expected to be in pseudo equilibrium with, and hence proportional to, the population of cells coinfecting with both the reporter genomes. Further, for time periods long compared to the lifetimes of infected cells and the characteristic timescale of the infection of uninfected cells, the production and death rates of infected cells are expected to exhibit a pseudo steady state. The number of cells infected with recombinant proviruses would then be proportional to the population of heterozygous virions and hence to the population of coinfecting cells, which may explain the origins of the second scaling relationship observed by Levy et al. [7]. (We present more mathematical arguments below.)

Whether currently available models of HIV dynamics that include infections by distinct viral genomes and recombination validate the above arguments and predict the observed scaling remains unclear. Dixit and Perelson predict the existence of the above scaling relationships under certain parameter regimes and, importantly, that the scaling relationships may depend on the length of time following the onset of infection [29]. In contrast, Levy et al. found that the scaling is independent of the time following the onset of infection [7]. Further, Levy et al. found that for the different initial viral loads employed, which varied well over two orders of magnitude, the parametric plots of different cell populations defining the scaling relationships superimpose remarkably tightly [7], whereas a similar superimposition at all times following the onset of infection is not apparent from the above scaling arguments, which hold after the establishment of pseudo equilibrium between viral production and clearance. A comprehensive model of HIV dynamics with recombination that quantitatively captures available experimental data is currently lacking.

In this work, we develop a detailed model of HIV dynamics that considers multiple infections of cells by distinct viral genomes and describes recombination. Our model captures several recent *in vitro* experimental findings quantitatively and provides key insights into the mechanisms underlying the emergence of recombinant forms of HIV. At the same time, our model is consistent with the standard model of viral dynamics, which successfully captures viral load changes in patients following the onset of antiretroviral therapy, and may therefore be extended to describe HIV dynamics with recombination *in vivo*.

Results

Model Formulation

We consider *in vitro* experiments where a population of uninfected CD4⁺ cells, T , is exposed simultaneously to two populations, V_{11} and V_{22} , of homozygous virions containing genomes 1 and 2, respectively. The genomes 1 and 2 are assumed to be distinct at two nucleotide positions, l_1 and l_2 , a distance l apart on the viral genome, with genome 1 having a mutation at position l_1 and genome 2 at l_2 (Figure 1A). Following exposure, target cells become infected singly or multiply with one of the genomes, or coinfecting with both genomes. Coinfecting cells produce heterozygous virions, V_{12} , which contain a copy each of genomes 1 and 2.

Infection of target cells by the virions V_{12} yields two kinds

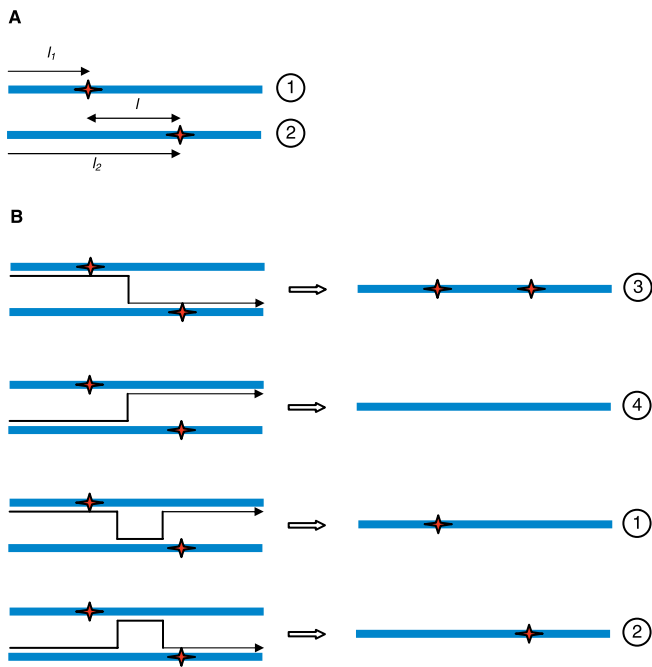


Figure 1. Schematic Representation of Viral Genomes and Recombination

Viral genomes 1 and 2 employed at the onset of infection (A) and the four genomes resulting from the recombination of genomes 1 and 2 (B). doi:10.1371/journal.pcbi.0030205.g001

of “recombinant” genomes depending on the template switching events during reverse transcription (Figure 1B). When the mutations at positions l_1 and l_2 are both included in the resulting proviral DNA, a recombinant genome that we denote as genome 3 is formed. When both the mutations are excluded, the other recombinant, genome 4, results. When one of the two mutations is included but not the other, genomes 1 and 2 are recovered. Thus, four kinds of viral genomes, 1, 2, 3, and 4, eventually infect cells.

We distinguish infected cells by the proviral genomes they contain. We denote by T_i cells containing a single provirus i , where $i \in \{1, 2, 3, 4\}$ represents the four genomes above. Thus, cells T_1 contain a single provirus 1, cells T_2 contain a single provirus 2, and so on. We denote by T_{ij} , where i and $j \in \{1, 2, 3, 4\}$, cells that contain two proviruses. Thus, cells T_{11} contain two copies of provirus 1, and cells T_{12} contain a copy of provirus 1 and a copy of provirus 2. Because cells T_{ij} are indistinguishable from cells T_{ji} , we subject i and j to the constraint $i \leq j$, resulting in ten kinds of doubly infected cells: $T_{11}, T_{12}, T_{13}, T_{14}, T_{22}, T_{23}, T_{24}, T_{33}, T_{34}$, and T_{44} . Extending the description, cells T_{ijk} are infected with three proviruses, and so on. Our aim is to describe the dynamics of recombination observed in experiments that employ two kinds of reporter viruses to infect cells. In these experiments, the number of cells infected with more than two genomes is estimated to be small [7]. Therefore, and for simplicity, we restrict our model to single and double infections of cells.

Random assortment of viral RNA produced in infected cells gives rise to ten different viral populations, which we denote V_{ij} , where $i \leq j$ and i and $j \in \{1, 2, 3, 4\}$, based on the viral genomes, i and j , contained in the virions. Thus, for instance, virions V_{34} contain a copy each of genomes 3 and 4. Cells infected with a single kind of provirus, T_i and T_{ii} , give

rise to homozygous virions, V_{ii} . Cells coinfecting with distinct proviruses, T_{ij} , produce the homozygous virions V_{ii} and V_{jj} and the heterozygous virions V_{ij} .

Below, we write equations to describe changes in the various cell and viral populations following the onset of infection.

Dynamical Equations

Uninfected cells. The in vitro dynamics of the uninfected cell population is governed by [29]

$$\frac{dT}{dt} = (\lambda - \mu)T - k_0TV, \tag{1}$$

where λ and μ are the proliferation and death rates of uninfected cells in vitro, k_0 is the second-order infection rate of uninfected cells, and $V = \sum_{j=i}^4 \sum_{i=1}^4 V_{ij}$ is the total viral load. Equation 1 is constrained by the initial condition that the uninfected cell population at the onset of infection ($t = 0$) is T_0 .

Infected cells. The singly infected cell subpopulations are determined by the integral equations:

$$T_i(t) = \int_0^t \left(k_0T(t-s) \sum_{h=j}^4 \sum_{j=1}^4 R_i(jh)V_{jh}(t-s) \right) \exp(-\delta s)M(i, t|s, t-s)ds. \tag{2a}$$

Here, $k_0T(t-s)V_{jh}(t-s)ds$ is the number of uninfected cells that are first infected by virions V_{jh} in an infinitesimal interval of time ds near time $t-s \geq 0$, where $t=0$ marks the onset of infection. We define $R_i(jh)$ as the probability that provirus i results from the recombination of genomes j and h , where i, j , and $h \in \{1, 2, 3, 4\}$ and $j \leq h$. Thus, $k_0T(t-s)R_i(jh)V_{jh}(t-s)ds$ is the expected number of uninfected cells first infected by virions V_{jh} in the interval ds near time $t-s$ and in which recombination results in provirus i . We assume that reverse transcription occurs rapidly following infection. Summation of $k_0T(t-s)R_i(jh)V_{jh}(t-s)ds$ over j and h therefore yields the total number of uninfected cells that are first infected with a single provirus i in the interval ds near $t-s$. The probability that these latter cells survive until time t is $\exp(-\delta s)$, where δ is the death rate of infected cells. We define $M(i, t | i, t-s)$ as the probability that a cell that is first infected with provirus i at time $t-s$ remains singly infected with the provirus i at time t given that the cell survives the intervening interval of duration s . The integrand in Equation 2a thus represents the number of uninfected cells that are first infected in the infinitesimal interval ds near time $t-s$ and survive with a single provirus i at time t . Integration over s from 0 to t gives the total number of cells containing a single provirus i at time t .

The doubly infected cell subpopulations are determined in an analogous manner:

$$T_{ii}(t) = \int_0^t \left(k_0T(t-s) \sum_{h=j}^4 \sum_{j=1}^4 R_i(jh)V_{jh}(t-s) \right) \exp(-\delta s)M(ii, t|s, t-s)ds, \tag{2b}$$

where $M(ii, t | i, t-s)$ is the probability that a cell that is first infected with provirus i at time $t-s$ contains an additional

provirus i at time t given that the cell survives the intervening interval of duration s .

For cells coinfecting with two different kinds of proviruses, we write

$$T_{ij}(t) = \int_0^t (k_0 T(t-s) \sum_{h=m}^4 \sum_{m=1}^4 R_i(hm) V_{hm}(t-s)) \exp(-\delta s) M(ij, t|i, t-s) ds + \int_0^t (k_0 T(t-s) \sum_{h=n}^4 \sum_{n=1}^4 R_j(hn) V_{hn}(t-s)) \exp(-\delta s) M(ji, t|j, t-s) ds \tag{2c}$$

where $i \neq j$ and $M(ij, t | i, t-s)$ is the probability that a cell that is first infected with provirus i at time $t-s$ contains an additional provirus j at time t given that the cell survives the intervening interval of duration s . The two integrals in Equation 2c correspond to the two ways of acquiring the two proviruses: i followed by j and j followed by i , respectively.

Multiple infections. To evaluate the conditional probabilities M , which characterize multiple infections, we consider a cell first infected with provirus i at time $t-s$. For times $\tau > t-s$, the rate of infection of the cell reduces exponentially because of CD4 down-modulation [28], so that [29]

$$k = k_0 \exp(-(\tau - t + s)/t_d), \tag{3}$$

where k_0 is the infection rate of an uninfected cell and t_d is the timescale of CD4 down-modulation. Three viral genes, *nef*, *env*, and *vpu*, acting via independent pathways, together induce nearly 100% down-modulation of CD4 molecules from the surface of an infected cell [26]. Of the three genes, the predominant influence is by *nef* [26], which induces rapid down-modulation of CD4 receptors following infection [28]. The latter down-modulation profile is well-described by an exponential decline (of timescale t_d) and is extended to include the influence of *env* and *vpu* [29]. How the susceptibility of a cell to new infections declines with CD4 down-modulation remains unknown. Here, we follow Dixit and Perelson [29] and assume that the infection rate k is directly proportional to the CD4 expression level and hence declines exponentially with time following the first infection.

Assuming that the cell, following its first infection with provirus i at time $t-s$, does not die, the probability that it contains the provirus i alone at time τ is by definition $M(i, \tau | i, t-s)$. In a subsequent infinitesimal interval $\Delta\tau$, in which at most one infection may occur, the probability that the cell is not infected is $(1 - kV(\tau)\Delta\tau)$, where k is given by Equation 3 and $V = \sum_{j=i}^4 \sum_{i=1}^4 V_{ij}$ is the total viral load. The probability that the cell remains singly infected with provirus i at time $\tau + \Delta\tau$ is therefore

$$M(i, \tau + \Delta\tau | i, t-s) = M(i, \tau | i, t-s) (1 - kV(\tau)\Delta\tau).$$

Subtracting $M(i, \tau | i, t-s)$, dividing by $\Delta\tau$, and letting $\Delta\tau \rightarrow 0$, we obtain

$$\frac{dM(i, \tau | i, t-s)}{d\tau} = -kV(\tau)M(i, \tau | i, t-s), \tag{4a}$$

with the initial condition that $M(i, t-s | i, t-s) = 1$.

Alternatively, a cell first infected with provirus i at time $t-s$ may contain two proviruses, i and j , at time $\tau + \Delta\tau$ if it contains

the provirus i alone at time τ and acquires an additional provirus j in the interval $\Delta\tau$, or if it contains both the proviruses i and j at time τ . (We ignore more than two infections of cells.) In the interval $\Delta\tau$, the probability that the cell acquires a second provirus j is $k\Delta\tau \sum_{m=h}^4 \sum_{h=1}^4 R_j(hm) V_{hm}(\tau)$ (see above), so that

$$M(ij, \tau + \Delta\tau | i, t-s) = M(i, \tau | i, t-s) k\Delta\tau \sum_{m=h}^4 \sum_{h=1}^4 R_j(hm) V_{hm}(\tau) + M(ij, \tau | i, t-s).$$

Subtracting $M(ij, \tau | i, t-s)$, dividing by $\Delta\tau$, and letting $\Delta\tau \rightarrow 0$, we obtain

$$\frac{dM(ij, \tau | i, t-s)}{d\tau} = kM(i, \tau | i, t-s) \sum_{m=h}^4 \sum_{h=1}^4 R_j(hm) V_{hm}(\tau), \tag{4b}$$

with the initial condition $M(ij, t-s | i, t-s) = 0$.

Substituting j by i in Equation 4b yields the corresponding evolution equation for $M(ii, \tau | i, t-s)$ with the initial condition $M(ii, t-s | i, t-s) = 0$.

Recombination. We next determine the probability $R_i(jh)$ that provirus i results from the recombination of genomes j and h . For homozygous virions, V_{ii} , reverse transcription yields the genome i alone so that

$$R_i(jj) = \begin{cases} 1 & i = j \\ 0 & i \neq j. \end{cases} \tag{5a}$$

(Note that we ignore mutations here.) For heterozygous virions, we consider first those combinations where the two genomes j and h differ in a single position, which happens when j is either 1 or 2 and h is either 3 or 4 (Figure 1B). Because the difference is in a single position, reverse transcription yields either of the two genomes with equal probability. Thus,

$$R_i(jh) = \begin{cases} 1/2 & i = j \text{ or } h \\ 0 & \text{otherwise} \end{cases} \text{ when } j \in \{1, 2\} \text{ and } h \in \{3, 4\}. \tag{5a}$$

Finally, when $j = 1$ and $h = 2$ and when $j = 3$ and $h = 4$, the two genomes differ in two positions; we consider these combinations explicitly. Let $j = 1$ and $h = 2$. Recall that genome 1 has a mutation at position l_1 and genome 2 at l_2 and that $l_2 - l_1 = l$ (Figure 1A). Recombination between genomes 1 and 2 yields genome 1 if the mutation on genome 1 is included in the resulting provirus and that on genome 2 is excluded (Figure 1B). Because reverse transcription is equally likely to begin on either genome, the probability that reverse transcriptase is on genome 1 at the position l_1 , i.e., the probability that the mutation on genome 1 is included in the resulting provirus, is 1/2. Given that the mutation on 1 is included, the mutation on 2 will be excluded if an even number of crossovers occurs between l_1 and l_2 .

Let n be the average number of crossovers during reverse transcription of the viral genome of length L . We define the crossover frequency, or the recombination rate, as $\rho = n/L$ crossovers per position. Assuming that crossovers occur independently, the probability $P(x)$ that x crossovers occur in a length l of the genome follows the Poisson distribution [14,30]

$$P(x) = \exp(-\rho l) \frac{(\rho l)^x}{x!},$$

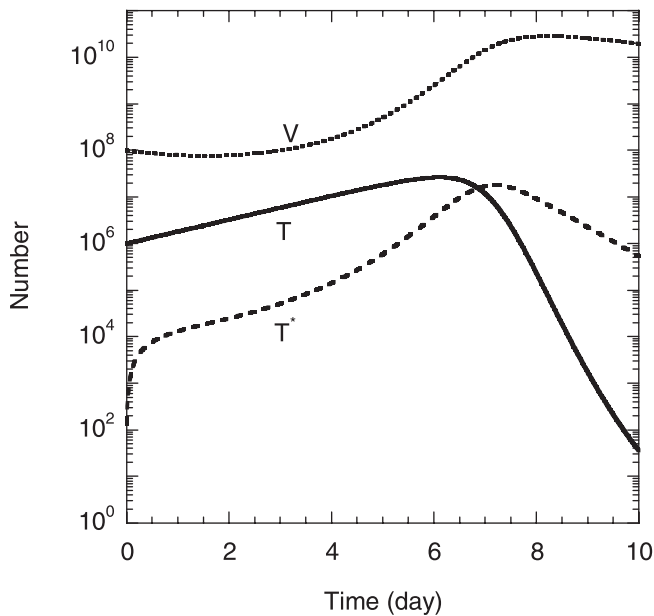


Figure 2. Model Predictions of the Overall Cell and Viral Dynamics
 The time evolution of the number of uninfected cells, T , the total number of infected cells, T^* , and the total viral load, V , following the onset of infection obtained by the solution of Equations 1–6 with the following parameter values: the initial target cell number, $T_0 = 10^6$; the initial viral load, $2V_0 = 10^8$; the birth and death rates of uninfected cells, $\lambda = 0.624 \text{ d}^{-1}$ and $\mu = 0.018 \text{ d}^{-1}$; the death rate of infected cells, $\delta = 1.44 \text{ d}^{-1}$; the viral burst size, $N = 1,000$; the clearance rate of free virions, $c = 0.35 \text{ d}^{-1}$; the infection rate constant of uninfected cells, $k_0 = 2 \times 10^{-10} \text{ d}^{-1}$; the CD4 down-modulation timescale, $t_d = 0.28 \text{ d}$; the recombination rate, $\rho = 8.3 \times 10^{-4}$ crossovers per position; and the separation between the mutations on genomes 1 and 2, $l = 408$ base pairs.
 doi:10.1371/journal.pcbi.0030205.g002

where $x! = x(x-1)\dots 2.1$. The probability that an even number of crossovers occurs in the length l is therefore the sum

$$\sum_{x=0,2,4,\dots} P(x) = \exp(-\rho l) \sum_{x=0,2,4,\dots} \frac{(\rho l)^x}{x!} = \exp(-\rho l) \cosh(\rho l).$$

Thus, the probability that genome 1 results from recombination of genomes 1 and 2 is

$$R_1(12) = \frac{1}{2} \exp(-\rho l) \cosh(\rho l). \tag{5c}$$

Similarly, genome 2 results from genomes 1 and 2 if the mutation on genome 1 is excluded and an even number of crossovers occurs between l_1 and l_2 so that the mutation on 2 is included. It follows that $R_2(12) = R_1(12)$.

Genome 3 results from genomes 1 and 2 if the mutation on genome 1 is included and an odd number of crossovers occurs between l_1 and l_2 so that the mutation on genome 2 is also included. Following the above arguments, we find that

$$R_3(12) = \frac{1}{2} \exp(-\rho l) \sinh(\rho l), \tag{5d}$$

and that $R_4(12) = R_3(12)$.

Similarly, when $j = 3$ and $h = 4$, we derive

$$R_1(34) = R_2(34) = \frac{1}{2} \exp(-\rho l) \sinh(\rho l), \tag{5e}$$

and

$$R_3(34) = R_4(34) = \frac{1}{2} \exp(-\rho l) \cosh(\rho l). \tag{5f}$$

Virions. Finally, we write equations for the time evolution of the various viral populations:

$$\frac{dV_{ii}}{dt} = N\delta \left(T_i + T_{ii} + \frac{1}{4} \sum_{j=i+1}^4 T_{ij} + \frac{1}{4} \sum_{h=1}^{i-1} T_{hi} \right) - cV_{ii} \tag{6a}$$

and

$$\frac{dV_{ij}}{dt} = \frac{1}{2} N\delta T_{ij} - cV_{ij}, i \neq j, \tag{6b}$$

where we recognize that cells T_i and T_{ii} produce homozygous virions V_{ii} , and cells T_{ij} produce homozygous virions V_{ij} and heterozygous virions V_{ij} in the proportions 1/4, 1/4, and 1/2, respectively. N is the viral burst size and δ is the death rate of infected cells, both assumed to be independent of the multiplicity of infection [29]. Equations 6a and 6b are constrained by the initial condition that the viral population at the onset of infection is composed of equal subpopulations of the homozygous virions V_{11} and V_{22} alone, i.e., $V_{11} = V_{22} = V_0$ at $t = 0$.

Equations 1–6 present a model of HIV dynamics with multiple infections of cells and recombination.

Model Predictions

We solve Equations 1–6 (Methods) using the following parameter estimates drawn from in vitro studies [29,31]: the birth and death rate of target cells, $\lambda = 0.624 \text{ d}^{-1}$ and $\mu = 0.018 \text{ d}^{-1}$; the death rate of infected cells, $\delta = 1.44 \text{ d}^{-1}$; the viral burst size, $N = 1,000$; and the clearance rate of free virions, $c = 0.35 \text{ d}^{-1}$. We let an initial target cell population, $T_0 = 10^6$, be exposed to two equal viral populations, $V_{11} = V_{22} = V_0$, which we vary over the experimental range, $2V_0 = 10^6$ to 10^{10} [7]. The infection rate constant, k_0 , the timescale of CD4 down-modulation, t_d , and the recombination rate, ρ , are not well-established, and we vary these parameters over ranges that define their best current estimates. We choose l , the separation between the mutations on genomes 1 and 2, in accordance with experiments (see below).

Virus and cell dynamics. In Figure 2, we present the time evolution of uninfected cells, T , the total infected cell population, $T^* = \sum_{i=1}^4 T_i + \sum_{j=i}^4 \sum_{i=1}^4 T_{ij}$, and the total viral load, $V = \sum_{j=i}^4 \sum_{i=1}^4 V_{ij}$, for the parameter values $2V_0 = 10^8$, $k_0 = 2 \times 10^{-10} \text{ d}^{-1}$, $t_d = 0.28 \text{ d}$, $\rho = 8.3 \times 10^{-4}$ crossovers per position (see below), and $l = 408$ base pairs. We find that T , T^* , and V evolve in two dominant phases, an initial rise and a subsequent fall. The initial rise in T is due to the net proliferation of uninfected cells at the rate $(\lambda - \mu)T$ (Equation 1), which in the initial stages of infection is large compared to the loss of uninfected cells by infection at the rate k_0VT . The latter infection process causes T^* to rise. The rise in T^* and hence viral production results in an increase in V . When V becomes large, the loss of uninfected cells by infection dominates cell proliferation and induces a decline in T . In Figure 2, T reaches a maximum at time $t \approx 6 \text{ d}$ after the onset of infection. The decline in T lowers the formation of infected cells and T^* decreases at the death rate δ . Finally, the loss of T^* lowers viral production and induces a decline in V at the clearance rate c . This overall two-phase dynamics is similar to the T cell dynamics observed in vitro [7].

In Figure 3A, we present the distribution of the infected cells, T^* , in Figure 2 into various singly and doubly infected cell subpopulations. We find that the various infected cell

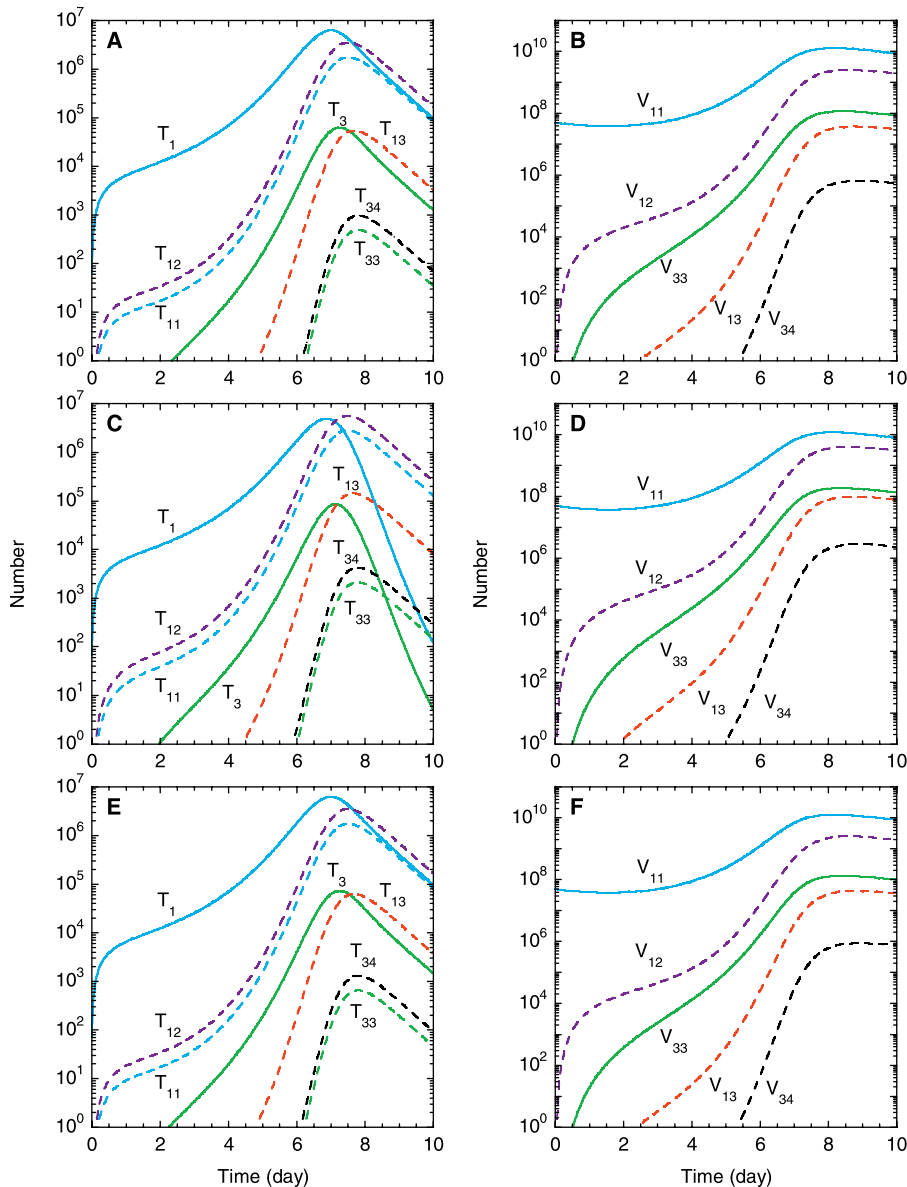


Figure 3. Model Predictions of the Dynamics of Different Infected Cell and Viral Subpopulations

The time evolution of the various singly (solid lines) and doubly (dashed lines) infected cell (left panels) and homozygous (solid lines) and heterozygous (dashed lines) viral subpopulations (right panels) following the onset of infection. Note that $T_1 = T_2$, $T_{11} = T_{22}$, $T_3 = T_4$, $T_{33} = T_{44}$, $T_{13} = T_{23} = T_{14} = T_{24}$, $V_{11} = V_{22}$, $V_{33} = V_{44}$, and $V_{13} = V_{23} = V_{14} = V_{24}$. The parameter values employed are the same as those in Figure 2 except that $t_d = 2.8$ d in (C) and (D) and $\rho = 10^{-3}$ crossovers per position in (E) and (F). doi:10.1371/journal.pcbi.0030205.g003

subpopulations also follow the two-phase dynamics above. The relative prevalence of the latter subpopulations is coupled to that of the corresponding viral subpopulations, which we present in Figure 3B. Because virions V_{11} and V_{22} alone are employed at the onset of infection, their numbers are larger than those of other viral subpopulations. When target cells are abundant, CD4 down-modulation ensures that singly infected cells occur more frequently than doubly infected cells. Thus, during the first phase of the dynamics following the onset of infection, cells singly infected with the infecting genomes, i.e., T_1 and T_2 , are the most prevalent. Note that because $V_{11} = V_{22} = V_0$ at the time of infection, at all subsequent times $T_1 = T_2$. Next in prevalence are cells infected twice with genome 1 and/or 2. Because coinfection by genomes 1 and 2 is twice as likely as double infection by either 1 or 2, cells T_{12} are more prevalent than T_{11} ($= T_{22}$).

The population of heterozygous virions, V_{12} , increases because of viral production from the coinfecting cells T_{12} .

Infections by V_{12} give rise to cells T_3 and T_4 , infected singly with the recombinant genomes, which in turn produce virions V_{33} and V_{44} , respectively. Coinfection by genomes 1 and 3 yields cells T_{13} , whose numbers are larger than those of the doubly infected cells T_{33} ($= T_{44}$) because of the small population of V_{33} compared to V_{11} . Again, because coinfection by genomes 3 and 4 is twice as likely as double infection by either 3 or 4, cells T_{34} are larger in number than T_{33} . Yet, homozygous virions V_{33} are more prevalent than heterozygous virions V_{34} because cells T_3 , T_{33} , and T_{34} produce V_{33} , whereas cells T_{34} alone produce V_{34} .

In the second dynamical phase, infected cell subpopulations decline because of cell death at rate δ . Singly infected

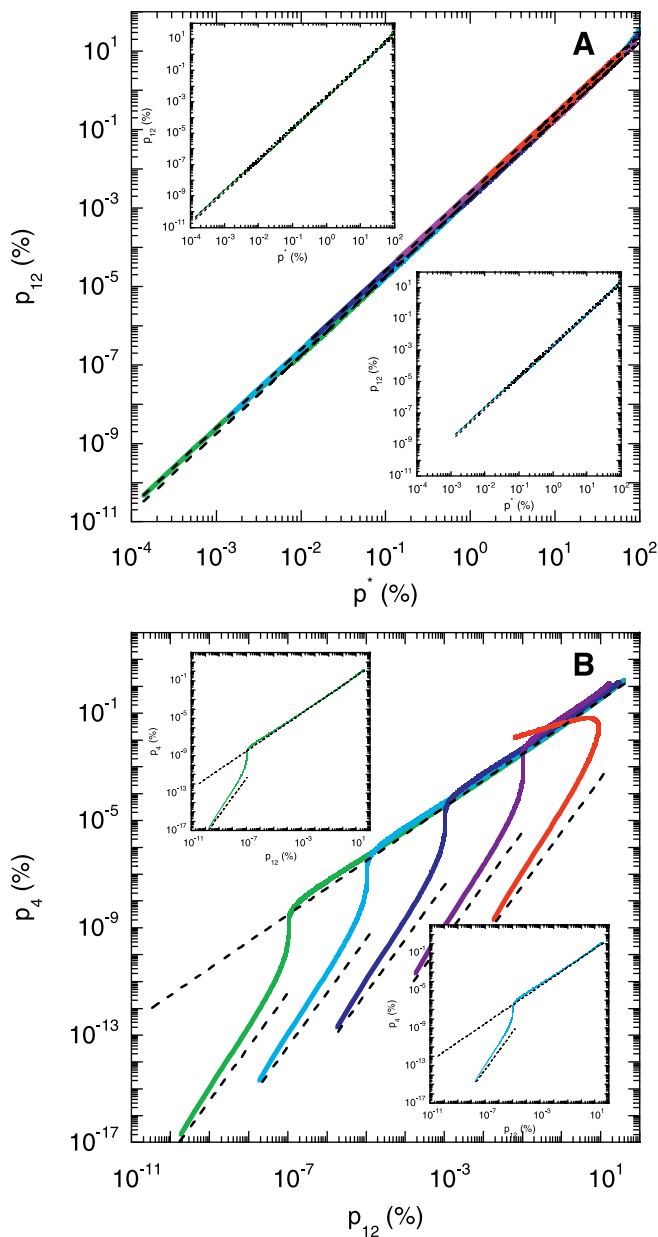


Figure 4. Model Predictions of Scaling Patterns

Parametric plots of (A) the percentage of cells coinfecting with genomes 1 and 2, p_{12} , versus the total percentage of infected cells, p^* , and (B) the percentage of cells infected with the recombinant 4, p_4 , versus p_{12} , obtained by solving Equations 1–6 for different initial viral loads, $2V_0 = 10^6$ (green), 10^7 (cyan), 10^8 (blue), 10^9 (purple), and 10^{10} (red). The dashed lines are scaling patterns predicted by Equation 7. The insets show the parametric plots for the individual cases, $2V_0 = 10^6$ (green) and 10^7 (cyan).

doi:10.1371/journal.pcbi.0030205.g004

cell subpopulations decline additionally because of second infections. Viral populations decline at the clearance rate c . The overall two-phase dynamics and the relative prevalence of various infected cell subpopulations are again in agreement with in vitro experiments [7].

Changes in the initial viral load, $2V_0$, or the infection rate, k_0 , do not alter the dynamics above qualitatively (unpublished data) [7,29]. Importantly, the CD4 down-modulation time-scale, t_d , does not influence the overall dynamics in Figure 2 (unpublished data). We assume here that viral production

from cells is independent of the number of infections cells suffer, which is expected when viral production is limited by cellular rather than viral factors. Changes in t_d then alter the distribution of infected cells into various multiply infected cell subpopulations but do not alter the total population of infected cells, T^* , or, consequently, the overall viral dynamics [29]. In Figure 3C and 3D, we present the calculations in Figure 3A and 3B with $t_d = 2.8$ d. A higher value of t_d implies slower CD4 down-modulation, which renders infected cells susceptible to further infections for longer durations and hence increases the relative prevalence of multiply infected cells. Accordingly, we find that doubly infected and co-infected cell subpopulations are higher in Figure 3C than in Figure 3A. (The faster decline of singly infected cells in the second phase in Figure 3C compared to that in Figure 3A is due to increased second infections in the former.) Correspondingly, the relative prevalence of heterozygous and recombinant virions increases upon increasing t_d (Figure 3B and 3D).

Interestingly, the recombination rate, ρ , also does not influence the dynamics in Figure 2 (unpublished data). We assume here that viral fitness is not affected by the mutations at the positions l_1 and l_2 . Consequently, an increase in ρ increases the relative prevalence of recombinant genomes in the viral population but not the total viral load or the frequency of multiple infections. In Figure 3E and 3F, we present the calculations in Figure 3A and 3B with $\rho = 10^{-3}$ crossovers per position. Note that the numbers of cells singly and doubly infected with genomes 1 and/or 2 are identical to those in Figure 3A, indicating that the frequency of multiple infections remains unaltered by the increase in ρ . The relative prevalence of cells infected with genomes 3 and 4, however, and that of the recombinant virions V_{33} ($= V_{44}$) is higher in Figure 3E and 3F than in Figure 3A and 3B, respectively, because of the enhanced frequency of recombination in the former.

Scaling. We examine next whether the above dynamics captures the scaling relationships between the different infected cell subpopulations observed experimentally [7]. In Figure 4A, we present parametric plots of the percentage of cells coinfecting with genomes 1 and 2, $p_{12} = 100T_{12}/(T^* + T)$, versus the total percentage of infected cells, $p^* = 100T^*/(T^* + T)$, for different initial viral loads and with the parameter values employed in Figure 2. Remarkably, we find that for all the initial viral loads considered, p_{12} is proportional to $(p^*)^2$. The scaling behavior is observed over the entire period of infection ($t = 10$ d) including both the phases of the overall dynamics of Figure 2. Further, the parametric plots of p_{12} versus $(p^*)^2$ for different viral loads are superimposed, in agreement with the robust scaling observed in experiments [7].

In Figure 4B, we present the corresponding variation of the percentage of cells infected with the recombinant 4, $p_4 = 100(T_4 + \sum_{i=1}^4 T_{i4})/(T^* + T)$, with the percentage of coinfecting cells, p_{12} . Interestingly, we find two scaling regimes. When p_{12} is small, p_4 is proportional to $(p_{12})^2$, and the parametric plots are distinct for different values of V_0 . For larger values of p_{12} , p_4 is linearly proportional to p_{12} and independent of V_0 . Thus, the parametric plots in the latter regime are again superimposed, as observed in experiments [7].

We explain the origins of the above scaling regimes by

considering two limiting scenarios in our model (Methods). First, for times small compared to the CD4 down-modulation timescale, i.e., $t \ll t_d$, and when changes in viral and cell numbers are small, we find that

$$p_{12} \approx \frac{1}{400} (p^*)^2 \text{ and } p_4 \approx \frac{R_4(12)N\delta T_0}{2400k_0V_0^2} (p_{12})^2. \quad (7a)$$

Second, for times large compared to the time required for viral load evolution to reach pseudo steady state, i.e., $t \gg t_{eq}$, we obtain

$$p_{12} \approx \frac{1}{400} \frac{k_1}{k_0} (p^*)^2 \text{ and } p_4 \approx \frac{R_4(12)}{4} p_{12}, \quad (7b)$$

where we define k_1 as the mean rate of the second infection of singly infected cells. As we show in Figure 4, Equations 7a and 7b capture the scaling regimes predicted by our simulations.

Remarkably, the scaling $p_{12} \approx \frac{1}{400} (p^*)^2$ (Equation 7a) is independent of model parameters and viral and cell numbers. Further, the quadratic scaling between p_{12} and p^* continues to hold for $t > t_{eq}$ (Equation 7b), with the proportionality constant lower than 1/400 by a factor k_1/k_0 . We notice thus that a transition from the small time ($t \ll t_d$) scaling, $p_{12} \approx \frac{1}{400} (p^*)^2$, to the large time ($t \gg t_{eq}$) scaling, $p_{12} \approx \frac{1}{400} \frac{k_1}{k_0} (p^*)^2$, occurs in the parametric plots in Figure 4A. The transition occurs at larger values of p^* with increasing initial viral load. We find that a value of $k_1 = 1.4 \times 10^{-10} \text{ d}^{-1}$ captures the long-time scaling for all initial viral loads considered. On the other hand, the scaling between p_4 and p_{12} for $t \ll t_d$, $p_4 \approx \frac{R_4(12)N\delta T_0}{2400k_0V_0^2} (p_{12})^2$, depends on model parameters and the initial viral load (Figure 4B). Interestingly, however, the linear scaling between p_4 and p_{12} , $p_4 \approx \frac{R_4(12)}{4} p_{12}$, for $t > t_{eq}$ is independent of the initial viral load.

For very large viral loads ($2V_0 \geq 10^{10}$) and/or infection rates ($k_0 \geq 2 \times 10^{-9} \text{ d}^{-1}$; unpublished data), we find that rapid infection and the consequent death of infected cells preempts the establishment of pseudo steady state between viral production and clearance in the first phase of infection, so that the linear scaling relationship between p_4 and p_{12} is not observed (Figure 4B). Below, we compare model predictions with experiments.

Comparison with Experiments

Available in vitro experiments, where cells are simultaneously exposed to two distinct kinds of viral genomes, may be segregated into two categories. First, single-round infection experiments employ replication-incompetent (heterozygous) virions to infect cells, and measure the fraction of cells that contain recombinant proviral genomes [3,7,13,14]. Second, viral dynamics experiments employ replication-competent (homozygous) virions and determine the time evolution of populations of cells infected with recombinant genomes [7]. We employ our description of the recombination probability (Equation 5) to predict data from single-round infection experiments and our entire model (Equations 1–6) to describe the latter viral dynamics experiments.

Single round of infection. We consider single-round infection experiments, where target cells are exposed to a mixed viral population comprising homozygous virions, V_{11} and V_{22} , and heterozygous virions, V_{12} , in the proportions 1/4, 1/4, and 1/2, respectively. Small viral loads are employed so that multiple infections of cells are rare. Following infection, cells in which recombinant proviruses result are identified.

Rhodes et al. [14] varied the separation l between the distinguishing mutations on genomes 1 and 2 (Figure 1A) and measured the fraction, f , of infected cells that contained the recombinant genome 4, which carries neither of the distinguishing mutations on genomes 1 and 2 (Figure 1B). Rhodes et al. report the latter fraction as a percentage of the theoretical maximum fraction, f_{max} , attained at arbitrarily large separations and/or recombination rates (see below). We reproduce the experimental data of Rhodes et al. in Figure 5A.

We estimate the percentage of cells infected with genome 4 in the experiments of Rhodes et al. as follows. We recognize that cells infected with heterozygous virions V_{12} alone may possess the recombinant provirus 4. With the above distribution of the viral subpopulations, the probability that an infection is due to a heterozygous virion is 1/2. Following infection by a heterozygous virion, the probability that recombination yields genome 4 is $R_4(12)$ (Equation 5). Thus, the fraction, f , of infected cells that contain genome 4 is expected to be $(1/2)R_4(12) = (1/4)\exp(-\rho l)\sinh(\rho l)$. This fraction attains a maximum value, f_{max} , of 1/8 (or 12.5%) as $\rho l \rightarrow \infty$. (When $\rho l \rightarrow \infty$, a large number of crossovers occurs between l_1 and l_2 ; the mutations at l_1 and l_2 are then selected independently, each with a probability 1/2, so that $R_4(12) \rightarrow 1/4$.) Thus, according to our model, $f/f_{max} = [(1/2)R_4(12)] / (1/8)$, which upon combining with Equation 5 yields

$$\frac{f}{f_{max}} = 2\exp(-\rho l)\sinh(\rho l). \quad (8)$$

We fit predictions of Equation 8 to the experimental data of f/f_{max} versus l using ρ as an adjustable parameter (Figure 5A). Our model provides a good fit to the data, representing a successful test of our description of the recombination probabilities $R_i(jh)$ (Equation 5). The best-fit estimate of $\rho = 8.3 \times 10^{-4}$ crossovers per position indicates that $n \approx 8$ crossovers occur on average (95% confidence interval: 6–10) in a genome of length $L = 9,700$ nucleotides. This estimate of n is in excellent agreement with a direct estimate from sequence analysis of ~ 7.5 crossovers in a genome of 9,700 nucleotides [7]. We employ the best-fit estimate of $\rho = 8.3 \times 10^{-4}$ crossovers per position in our calculations above.

Levy et al. [7] also performed single-round infection experiments, where they exposed target cells simultaneously to homozygous reporter viruses containing either the cyan fluorescent protein (CFP) gene or the yellow fluorescent protein (YFP) gene, and heterozygous viruses with one strand containing the CFP gene and the other the YFP gene. The CFP and YFP genes were obtained by introducing specific mutations in the green fluorescent protein (GFP) gene. Thus, recombination events between the CFP and YFP genes that omit both the CFP and the YFP mutations yield the GFP gene. In addition, Levy et al. [30] observed that the CFP gene has certain distinguishing mutations between nucleotide positions ~ 440 and ~ 500 . When recombination includes both the critical CFP and YFP mutations, and also the latter distinguishing mutations on the CFP gene, the resulting genome exhibits green fluorescence. When the latter mutations are not included, however, the resulting genomes remain undetected. Levy et al. determined the percentage of infected cells that exhibited green fluorescence as a measure of the recombination rate.

To compare the observations of Levy et al. with our model

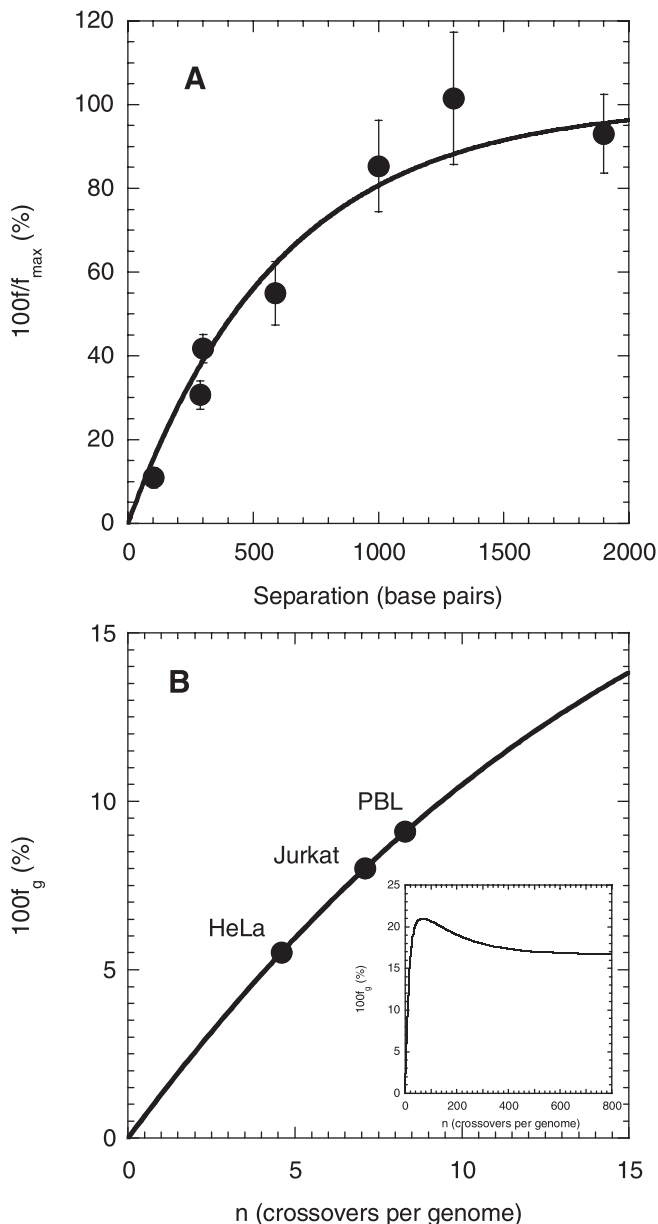


Figure 5. Comparisons of Model Predictions with Data from Single-Round Infection Experiments

(A) The ratio of the percentage of cells infected with the recombinant 4, f , and the theoretical maximum percentage, f_{\max} , as a function of the separation, l , between the mutations on genomes 1 and 2 (see Figure 1) determined by Rhodes et al. [14] (circles) and by Equation 8 (line) with $p = 8.3 \times 10^{-4}$ crossovers per position.

(B) The percentage of GFP⁺ cells as a function of the crossover frequency, n , determined by Equation 9 (line), on which are mapped the experimental percentages (circles) obtained by Levy et al. [7] with HeLa CD4, Jurkat, and primary T cells (PBL). The inset shows the prediction of Equation 9 over a larger range of values of n . doi:10.1371/journal.pcbi.0030205.g005

predictions, we let genome 1 (Figure 1A) represent the reporter virus with the CFP gene carrying the critical CFP mutation at $l_1 = 201$ and genome 2 the virus with the YFP gene carrying the critical YFP mutation at $l_2 = 609$, so that $l = l_2 - l_1 = 408$ [7]. We redefine genome 4 to encompass all genomes capable of green fluorescence. Thus, genome 4 includes genomes with the GFP gene, which contains neither of the mutations at l_1 and l_2 , and also those genomes that

contain both the mutations at l_1 and l_2 and the contents of genome 1 from positions 440 to 500. Accordingly, genome 3 includes those genomes that carry both the mutations at l_1 and l_2 but not all of the contents of genome 1 from positions 440 to 500. With these definitions of genomes 3 and 4, we recalculate the recombination probabilities of Equation 5d and find

$$R_4(12) = \frac{1}{2} \exp(-\rho l) \sinh(\rho l) + \frac{1}{2} \exp(-\rho l) \cosh(\rho l_a) \sinh(\rho l_b). \quad (9a)$$

The first term on the right-hand side of Equation 9a is the probability that recombination excludes both the mutations at l_1 and l_2 and is given by Equation 5d. The second term represents the contribution to $R_4(12)$ that arises from recombination events that include both the mutations at l_1 and l_2 and the contents of genome 1 from positions 440 to 500. The latter contribution is determined as follows. The probability that reverse transcription begins on genome 1 at position $l_1 = 201$ is $1/2$. Given that the mutation at l_1 is included, reverse transcriptase would be on genome 1 at position 440 if an even number of crossovers occurred between positions l_1 and 440, which happens with the probability $\exp(-\rho l_a) \cosh(\rho l_a)$, where $l_a = 440 - l_1$. For the contents of genome 1 between positions 440 and 500 to be included in the resulting provirus, no crossovers must occur between positions 440 and 500, the probability of which is $\exp(-\rho 60)$. Finally, the mutation at $l_2 = 609$ on genome 2 is included if an odd number of crossovers occurs between positions 500 and l_2 , which happens with the probability $\exp(-\rho l_b) \sinh(\rho l_b)$, where $l_b = l_2 - 500$. Multiplying the latter probabilities and recognizing that $l_a + l_b + 60 = l$ yields the second contribution to $R_4(12)$ above. Similarly, we find that

$$R_3(12) = \frac{1}{2} \exp(-\rho l) \sinh(\rho l) - \frac{1}{2} \exp(-\rho l) \cosh(\rho l_a) \sinh(\rho l_b). \quad (9b)$$

We determine the fraction of infected cells that fluoresce following exposure of cells to homozygous CFP and YFP virions and heterozygous CFP/YFP virions in the proportions $1/4$, $1/4$, and $1/2$, respectively, as follows. (Fluorescent cells are detected in the experiments as infected.) When single infections of cells predominate, half of the infections are due to homozygous virions, which cause cells to fluoresce regardless of recombination. The other half of the infections, which are due to heterozygous virions, induce fluorescence when recombination yields genome 1, 2, or 4. Levy et al. ignore GFP⁺ cells in their estimate of the total fraction of infected cells [30]. The latter fraction is thus $1/2 + (1/2)(R_1(12) + R_2(12))$. The experimentally determined fraction, f_g , of infected cells that are GFP⁺ is therefore $(1/2)R_4(12)/[(1/2) + (1/2)(R_1(12) + R_2(12))]$, which simplifies to

$$f_g = R_4(12)/[2 - R_3(12) - R_4(12)], \quad (9c)$$

where $R_3(12)$ and $R_4(12)$ are determined using Equations 9a and 9b, respectively.

Levy et al. [7] report the mean percentage of infected cells that are GFP⁺ to be 8.0 with Jurkat T cells, 5.5 with HeLa CD4 cells, and 9.1 with primary CD4⁺ T cells. We compare these percentages with our prediction of f_g and estimate the recombination rate in the respective cell types (Figure 5B). We find that the mean number of crossovers in a genome of

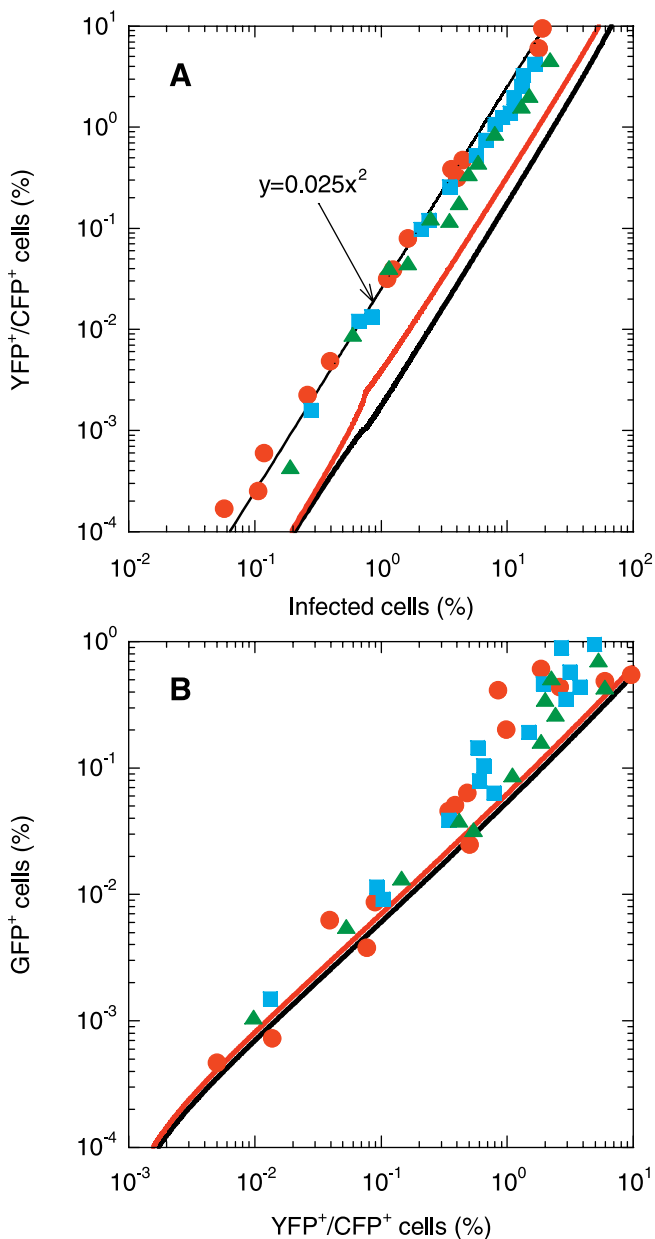


Figure 6. Comparisons of Model Predictions with Experimental Scaling Relationships

Model predictions (thick lines) obtained by solving Equations 1–6, but with Equation 5d replaced by Equations 9a and 9b, compared with experimental scaling relationships (symbols) between (A) the percentage of coinfecting cells (YFP^+/CFP^+) and the total percentage of infected cells, and (B) the percentage of GFP^+ cells and the percentage of coinfecting cells. The different symbols represent experiments conducted with cells from different donors [7]. Parameters employed for calculations are identical to those in Figure 2 except that for the red lines $t_d = 2.8$ d in (A) and $\rho = 10^{-3}$ crossovers per position in (B). The thin black line in (A) is the experimental best-fit line [7].
doi:10.1371/journal.pcbi.0030205.g006

9,700 nucleotides is 7.1 in Jurkat T cells, 4.6 in HeLa CD4 cells, and 8.3 in primary $CD4^+$ T cells. Direct sequence analysis from Jurkat T cells showed a mean crossover frequency of 7.5 (range 3–13) [7], in excellent agreement with the estimate obtained here and from our analysis of the experiments of Rhodes et al. [14] above. Whereas the mean

crossover frequency in HeLa cells is lower, that in primary $CD4^+$ T cells is again in excellent agreement with the estimate for Jurkat T cells and that from the data of Rhodes et al. [14].

With macrophages, Levy et al. [7] found that $\sim 29\%$ of infected cells are GFP^+ . We note that f_g defined in Equation 9c is a non-monotonic function of ρ : increasing ρ increases the probability of the accumulation of both the critical YFP and CFP mutations at l_1 and l_2 but lowers the probability that no crossovers occur between the positions 440 and 500 on genome 1. As a result, the second contribution to $R_4(12)$ in Equation 9a increases first and then decreases upon increasing ρ . Thus, upon increasing ρ , f_g increases ($f_g = 0$ when $\rho = 0$), reaches a maximum value of $\sim 21\%$ at $\rho = 0.007$ crossovers per position (~ 68 crossovers in 9,700 nucleotides), and declines to an asymptotic value of $\sim 16.7\%$ as $\rho \rightarrow \infty$ (Figure 5B, inset). The 29% GFP^+ cells observed with macrophages is thus higher than the maximum value of f_g predicted by our model. We note that a higher percentage of GFP^+ cells than the theoretical maximum of $\sim 21\%$ may result if cells are multiply infected, which we ignore in our description of single-round infection experiments. Indeed, Levy et al. [30] observed that a large percentage of macrophages are coinfecting despite the low viral loads employed. (Levy et al. reanalyzed their experiments [7] by accounting for double and triple infections of cells and estimated ρ [30]; the differences in their estimates of ρ and our estimates above may be attributed to the occurrence of multiple infections, which we ignore.) In contrast, Chen et al. and Rhodes et al. found no significant distinction between different cell types in their experiments [13,14]. Whether nonrandom infection processes [4,5] favored enhanced multiple infections of macrophages in the experiments of Levy et al. [7] remains to be ascertained.

Dynamics and scaling. We next compare our predictions with the dynamical and scaling patterns that Levy et al. [7] observed in their experiments with replication-competent viruses. Levy et al. employed equal populations of homozygous CFP and YFP reporter viruses to infect $\sim 10^6$ $CD4^+$ T cells and detected the total percentage of cells infected (i.e., that fluoresced), p^* , the percentage of cells that were coinfecting with CFP and YFP genomes, p_{12} , and the percentage of cells that were GFP^+ , p_4 , with time following the onset of infection. The quantities evolved in two distinct phases—an initial rise and a subsequent fall. Our model captures the two-phase dynamics qualitatively, as we demonstrate in Figure 4 (see “Model Predictions” above), and elucidates the origins of the two phases and of the observed relative prevalence of different infected cell subpopulations. Quantitative comparisons with the dynamical data are precluded by the possible presence in the experimental cultures of cells not susceptible to infection, which we discuss below. We focus here on the corresponding scaling relationships observed by Levy et al. [7]. In Figure 6A, we reproduce the experimental scaling relationship observed between p_{12} and p^* , and in Figure 6B, the relationship between p_4 and p_{12} .

In Figure 6, we also present model predictions of p_{12} versus p^* and p_4 versus p_{12} for the initial viral load $2V_0 = 10^8$ and with the parameters employed in Figure 4. In the calculations in Figure 6, however, we replace Equation 5d for $R_3(12)$ and $R_4(12)$ by Equations 9a and 9b and ignore cells infected with genomes 3 alone, i.e., T_3 and T_{33} , in our count of the total number of infected cells, T^* , because the latter cells do not

fluoresce and remain undetected in the experiments [7]. We recognize that unlike in single-round infection experiments, the other recombination probabilities involving genome 4, $R_i(j4)$ in Equation 5 must also be altered to differentiate between the two kinds of GFP⁺ genomes (see above) present in the experiments. Based on the relative magnitudes of the two contributions to $R_4(12)$ in Equation 9a (for $\rho = 8.3 \times 10^{-4}$ crossovers per position, the values of the two terms are ~ 0.12 and ~ 0.03 , respectively), we expect, however, that a majority of the GFP⁺ genomes are those that contain neither of the mutations on genomes 1 and 2, i.e., as shown in Figure 1B. We therefore employ, as an approximation, the remaining recombination probabilities as defined in Equation 5.

We find that our model captures the quadratic scaling, $p_{12} \sim (p^*)^2$, qualitatively. Our model predicts that for small values of p^* , the scaling relationship $p_{12} \approx \frac{1}{400}(p^*)^2$ holds (Equation 7a), and that it transitions to $p_{12} \approx \frac{k_1}{k_0} \frac{1}{400}(p^*)^2$ for larger values of p^* (Equation 7b). Because $k_1/k_0 < 1$, the parametric plot of p_{12} versus p^* exhibits a parallel shift to lower values of p_{12} at large values of p^* . Indeed, this shift is also observed in experiments, where the data lie on the experimental best-fit scaling relationship, $p_{12} \approx \frac{1}{40}(p^*)^2$, for small p^* , but below the best-fit line for large p^* .

Quantitatively, our model underpredicts the percentage of coinfecting cells p_{12} compared to the experiments: the experimental proportionality constant relating p_{12} and p^* , 1/40, is an order of magnitude larger than that estimated by our model, 1/400. One reason for this discrepancy might be the presence in the experimental cultures of cells not susceptible to infection. Hypothesize, for instance, the presence of a population, T_{ns} , of non-susceptible cells in culture. The percentage of infected cells, p^* , then becomes $100T^*/(T^* + T + T_{ns})$, where T is now the susceptible target cell population governed by Equation 1, and T^* is the total population of infected cells. Similarly, the percentage of coinfecting cells, p_{12} , becomes $100T_{12}/(T^* + T + T_{ns})$. The resulting proportionality constant, $p_{12}/(p^*)^2 = \frac{T_{12}}{(T^*)^2} \frac{T^* + T + T_{ns}}{100}$ is greater than that determined by our model ($T_{ns} = 0$) by the factor $1 + T_{ns}/(T^* + T)$. An estimate of the latter factor is obtained by noting that the maximum percentage of cells infected in experiments is $\sim 20\%$ for the two highest initial viral loads employed [7]. At the peak infection, we may assume that nearly all susceptible cells are infected, i.e., $T \approx 0$, so that $T^*/(T^* + T_{ns}) \approx 1/5$. Thus, the factor above, $1 + T_{ns}/T^* \approx 5$, explains at least in part the difference between the experimental proportionality constant and that derived from our model. Further, uncertainties exist in our knowledge of the CD4 down-modulation timescale, t_d , of the cells in culture [26,28,29]. A larger value of t_d may enhance the frequency of multiple infections and increase p_{12} for a given value of p^* . Indeed, our model predictions assuming $t_d = 2.8$ d appear to be in better agreement with the experimental scaling between p_{12} and p^* (Figure 6A). We note, however, that $t_d = 2.8$ d implies that $k_1 \approx k_0$ throughout, so that several assumptions underlying the scaling relations in Equation 7 are not expected to hold. In particular, we find that for large p^* , the proportionality constant relating p_{12} and p^* is higher than 1/400, the value of the constant for small p^* , in contrast to that predicted for smaller values of t_d and observed in the experimental data. Nonetheless, quantitative comparison with the experimental scaling between p_{12} and p^* requires a description of the dynamics of the non-susceptible cell

population including possible transitions from non-susceptibility to susceptibility and vice versa due to stimulation by regular IL-2 addition and loss of cell activation, respectively, which is beyond the scope of the present paper.

The presence of non-susceptible cells, however, does not influence the linear scaling relationship between p_{12} and p_4 . Given that $p_4 = 100(T_4 + \sum_{i=1}^4 T_{i4})/(T^* + T + T_{ns})$, the proportionality constant for the linear scaling, $p_4/p_{12} \approx \frac{T_4 + \sum_{i=1}^4 T_{i4}}{T_{12}}$, is independent of T_{ns} . Our model predicts that for small p_{12} , p_4 is proportional to $(p_{12})^2$ and for large p_{12} , p_4 is proportional to p_{12} (Equation 7; Figure 4B). In the experiments, the quadratic scaling at small p_{12} is not observed [7]. For low initial viral loads, the transition from the quadratic to the linear scaling regime occurs at small values of p_{12} that may lie below experimental detection limits (Figure 4B). Upon increasing the initial viral load, the value of p_{12} at the transition increases but the quadratic scaling is short-lived. Thus, for larger viral loads, the transition to the linear scaling regime appears to occur before the first measurement following the onset of infection is made (at $t \approx 2$ d). Consequently, the linear scaling regime may alone be accessed in experiments.

We find remarkably that our model quantitatively captures the experimental linear scaling between p_4 and p_{12} (Figure 6B). For small values of p_{12} , the model is in excellent agreement with the data. Interestingly, the same recombination rate ($n = 8$ crossovers in a genome of 9,700 nucleotides) obtained from single-round infection experiments is employed in the latter predictions. (The latter predictions, however, are not adequately sensitive to changes in the recombination rate; calculations with a higher recombination rate, $\rho = 0.001$ crossovers per position [$n = 10$ crossovers in a genome of 9,700 nucleotides], yield only a marginal improvement in the comparison between model predictions and experiment [Figure 6B].) For large values of p_{12} , the model slightly underpredicts the experimental data, possibly because of the increased likelihood of more than two infections of cells, which we ignore. Nonetheless, the quantitative agreement between model predictions and the experimental scaling relationship and the consistency of the predictions with the recombination rate estimated from independent single-round infection assays indicate that our model accurately captures the underlying dynamics of recombination during HIV infection.

Discussion

The emergence of recombinant forms of HIV that are resistant to multiple drugs often underlies the failure of current antiretroviral therapies for HIV infection. Yet, the dynamics of the emergence of recombinant genomes in individuals infected with HIV remains poorly understood. Current models of HIV dynamics are unable to explain available experimental data of the frequency of occurrence and the time evolution of recombinant HIV genomes quantitatively. We developed a model that describes the dynamics of the emergence of recombinant forms of HIV and quantitatively captures key experimental observations. Mimicking recent experiments [5,7,14], we considered target cells exposed simultaneously to two kinds of homozygous virions. We constructed integral equations that predict the time evolution of the population of cells coinfecting with both

kinds of viruses. Following the first infection of a cell, viral gene expression induces CD4 down-modulation, which lowers the susceptibility of the cell to further infections. Because cells are infected asynchronously, determination of the frequency of multiple infections requires accounting for the different susceptibilities of individual cells to further infections at any given time based on the different times elapsed from their respective first infections, which is accomplished by the integral equation formalism [29]. Coinfected cells produce heterozygous progeny virions, which infect cells and yield recombinant proviral genomes. We developed a probabilistic description of template switching during reverse transcription and predicted the frequency with which heterozygous virions give rise to recombinant genomes. We integrated our descriptions of multiple infections of cells and recombination into standard models of HIV dynamics [15–17] and formulated dynamical equations that predict the time evolution of the populations of uninfected, singly infected, and multiply infected cells, and of homozygous, heterozygous, and recombinant viruses.

Model predictions are in agreement with the T cell dynamics observed *in vitro*. Levy et al. [7] found that following the onset of infection, the infected cell subpopulations evolve in two phases, an initial rise and a subsequent fall. Further, the percentage of cells infected by recombinant genomes, p_4 , is a small fraction of the percentage of coinfecting cells, p_{12} , which in turn is a small fraction of the total percentage of cells infected, p^* . The two-phase dynamics and the relative prevalence of various infected cell subpopulations are in agreement with our model predictions. Our model also captures the scaling patterns relating the frequency of infection, coinfection, and recombination observed experimentally. Levy et al. [7] found remarkably that p_{12} is proportional to $(p^*)^2$ and that p_4 is proportional to p_{12} , independent of the initial viral load and the time following the onset of infection. Our model predicts both these scaling patterns and that the patterns are independent of the initial viral load and the time following the onset of infection. Quantitative comparison between our model predictions and the experimental scaling relationship between p_{12} and $(p^*)^2$ is precluded by the poorly characterized dynamics of cells not susceptible to infection by HIV that may be present in the experimental cultures. We showed, however, that the presence of non-susceptible cells does not influence the linear scaling relationship between p_4 and p_{12} . Indeed, our model predictions are in quantitative agreement with the experimental scaling relationship between p_4 and p_{12} . The quantitative agreement indicates that our model captures the underlying dynamics of HIV recombination accurately.

Our model also captures data from single-round infection experiments on the frequency of the accumulation by recombination of distinct mutations present on the two RNA strands within a virion. From comparisons of model predictions with the experiments of Rhodes et al. [14], we estimate that ~ 8 template switches, or crossovers, occur on average (95% confidence interval: 6–10) during the reverse transcription of an entire HIV genome of $\sim 10^4$ nucleotides. This number is in agreement with independent estimates from direct sequence analysis by Levy et al. [7], who observed ~ 7.5 crossovers (range 3–13) on average. Comparison of our

model predictions with the single-round infection assays performed by Levy et al. yields crossover frequencies of ~ 7.1 in Jurkat T cells, ~ 4.6 in HeLa CD4 cells, and ~ 8.3 in primary CD4⁺ T cells. Whereas the crossover frequency in HeLa cells is lower, the frequency in the other two cell types is in agreement with the estimate obtained from our analysis of the experiments of Rhodes et al. [14]. Further, the scaling relationship between p_4 and p_{12} described above is also consistent with a recombination rate of ~ 8 crossovers per $\sim 10^4$ nucleotides.

The power law scaling that the number of doubly infected cells is proportional to the square of the total number of infected cells is also predicted by the model of HIV dynamics with multiple infections developed by Dixit and Perelson [29]. In contrast to experiments, however, the predicted scaling is dependent on the time following the onset of infection and the initial viral load. Here, by considering percentages rather than numbers of infected cells and by distinguishing between cells doubly infected by a single kind of genome and coinfecting with distinct genomes, we mimic experimental quantities more accurately and find that the scaling relationship is independent of the time following infection or the initial viral load, as observed in experiments [7]. Fraser argues that the quadratic scaling observed between the percentage of doubly infected cells and the total percentage of infected cells, the latter predominantly singly infected, may imply a deviation from mass action kinetics for the second (and perhaps further) infections of cells and suggests, motivated by the scaling, that the rate of second infection of cells may be proportional to the square of the viral load ($r \sim kV^2$) [22]. Here, we find that the quadratic scaling emerges without deviations from mass action kinetics ($r \sim kV$). Further, to address possible differences between the rates of first, second, and third infections, due, for instance, to CD4 down-modulation, Fraser postulates the use of different values of the rate constants, k , for successive infections. In our model, the differences in the rate constants for multiple infections follow naturally from our description of CD4 down-modulation (Equation 3). The latter description facilitates accurate estimation of the frequency of multiple infections under varying viral loads: when the viral load is high, for instance, the second infection of a cell may occur rapidly after its first infection, in which case the rate constants for the first and second infections are expected to be similar due to negligible CD4 down-modulation in the intervening interval. A fixed rate constant for second infection (independent of the viral load) would then tend to underestimate the frequency of double infections. The dependence on the viral load of the variation of the apparent infection rate constant with the number of infections implies that when viral load changes are rapid, the likelihood of a cell suffering multiple infections would depend on the instant of its first infection. For instance, in patients undergoing efficacious antiretroviral therapy, a cell first infected at the start of therapy, when the viral load is large, is expected to have a higher rate constant for second infection than a cell that is first infected a day after the onset of therapy, when the viral load is significantly reduced. Our integral equation formalism, which accounts for the asynchronous first infections of cells, allows accurate determination of the frequency of multiple infections and consequently the influence of recombination throughout the infection period.

If the distinction between different viral genomes is ignored, our model reduces to the model of HIV dynamics with multiple infections developed by Dixit and Perelson [29] when more than two infections of cells are rare. Indeed, changes in the total viral load, target cell numbers, and total infected cell numbers predicted by our model (Figure 2) are identical to those predicted by the latter model. Importantly, the latter model reduces to the standard model of HIV dynamics [15–17] when viral production from cells is independent of the number of infections cells suffer. Our model is thus consistent with the standard model of HIV dynamics, which successfully predicts viral load changes in patients following the onset of antiretroviral therapy [15–17]. Further, infections in SCID-hu mice also show scaling patterns similar to those observed in vitro [7] and predicted by our model, reinforcing the notion that our model may be applied to describe the dynamics of recombination in vivo.

Several advances of our model are essential, however, to predict the emergence of recombinant genomes in vivo. First, that infected splenocytes from two HIV patients harbored 3–4 proviruses per cell on average [6] suggests that multiple infections of cells may be more prevalent in vivo than is assumed in our model. Second, multiple infections in vivo may be orchestrated by cell–cell transmission as well as by free virions [32,33]. Third, HIV has a high mutation rate [34], which introduces genomic variations in vivo that may subsequently be accumulated by recombination. Indeed, the high mutation and turnover rates of HIV in vivo [17,35] suggest that the likelihood of the preexistence of individual drug resistance mutations in patients is high [36]: approximately half of the HIV patients in the United States are estimated to be infected with genomes that possess resistance to at least one of the currently available drugs [37]. Our model describes how preexisting mutations may become associated by recombination. Determination of the existence of individual mutations, however, requires a description of the HIV mutation process, which we ignore. Fourth, fitness interactions between mutations [24] modulate the relative prevalence of recombinant genomes, whereas we assume all viral genomes to be equally fit. We note that incorporating fitness selection enables our present model to describe additionally in vitro serial passage experiments of the emergence of drug resistance via recombination [2,38]. Finally, whereas we consider two loci, a description of recombination between more than two loci is essential in vivo, as more than two mutations are typically responsible for resistance to individual drugs [37]. With the above advances, some of which are suggested in currently available models [18,20,22,23], our model may facilitate prediction of the emergence of multi-drug-resistant strains of HIV in infected individuals.

Methods

Solution of dynamical equations. We non-dimensionalize Equations 1–4 and 6 using the following dimensionless quantities:

$$\begin{aligned} \tilde{T} &= \frac{T}{T_0}, \tilde{T}_i = \frac{T_i}{T_0}, \tilde{T}_{ii} = \frac{T_{ii}}{T_0}, \tilde{T}_{ij} = \frac{T_{ij}}{T_0}, \tilde{V}_{ij} = \frac{V_{ij}}{k_0 V_0}, \tilde{t} = \delta t, \tilde{\tau} = \delta \tau, \tilde{s} = \delta s, \\ \tilde{t}_d &= \delta t_d, \Xi = \frac{c}{\delta}, \Lambda = \frac{\lambda - \mu}{\delta}, \Omega = \frac{k_0 V_0}{\delta}, \Gamma = \frac{NT_0}{V_0} \end{aligned} \tag{10}$$

and obtain

$$\frac{d\tilde{T}}{d\tilde{t}} = \Lambda \tilde{T} - \Omega \tilde{V} \tilde{T}, \tag{11}$$

$$\tilde{T}_i(\tilde{t}) = \Omega \int_0^{\tilde{t}} \left(\tilde{T}(\tilde{t} - \tilde{s}) \sum_{h=j}^4 \sum_{j=1}^4 R_i(jh) \tilde{V}_{jh}(\tilde{t} - \tilde{s}) \right) \exp(-\tilde{s}) M(i, \tilde{t}|i, \tilde{t} - \tilde{s}) d\tilde{s}, \tag{12a}$$

$$\tilde{T}_{ii}(\tilde{t}) = \Omega \int_0^{\tilde{t}} \left(\tilde{T}(\tilde{t} - \tilde{s}) \sum_{h=j}^4 \sum_{j=1}^4 R_i(jh) \tilde{V}_{jh}(\tilde{t} - \tilde{s}) \right) \exp(-\tilde{s}) M(ii, \tilde{t}|i, \tilde{t} - \tilde{s}) d\tilde{s}, \tag{12b}$$

$$\begin{aligned} \tilde{T}_{ij}(\tilde{t}) &= \Omega \int_0^{\tilde{t}} \left(\tilde{T}(\tilde{t} - \tilde{s}) \sum_{h=m=1}^4 \sum_{h=m=1}^4 R_i(hm) \tilde{V}_{hm}(\tilde{t} - \tilde{s}) \right) \exp(-\tilde{s}) M(ij, \tilde{t}|i, \tilde{t} - \tilde{s}) d\tilde{s} \\ &+ \Omega \int_0^{\tilde{t}} \left(\tilde{T}(\tilde{t} - \tilde{s}) \sum_{h=m=1}^4 \sum_{h=m=1}^4 R_j(hm) \tilde{V}_{hm}(\tilde{t} - \tilde{s}) \right) \exp(-\tilde{s}) M(ji, \tilde{t}|j, \tilde{t} - \tilde{s}) d\tilde{s} \end{aligned} \tag{12c}$$

$$\tilde{k} = \exp(-(\tilde{\tau} - \tilde{t} + \tilde{s})/\tilde{t}_d), \tag{13}$$

$$\frac{dM(i, \tilde{\tau}|i, \tilde{t} - \tilde{s})}{d\tilde{\tau}} = -\Omega \tilde{k} \tilde{V}(\tilde{\tau}) M(i, \tilde{\tau}|i, \tilde{t} - \tilde{s}), \tag{14a}$$

$$\frac{dM(ij, \tilde{\tau}|i, \tilde{t} - \tilde{s})}{d\tilde{\tau}} = \Omega \tilde{k} \sum_{m=h}^4 \sum_{h=1}^4 R_i(hm) \tilde{V}_{hm}(\tilde{\tau}) M(ij, \tilde{\tau}|i, \tilde{t} - \tilde{s}), \tag{14b}$$

$$\frac{d\tilde{V}_{ii}}{d\tilde{t}} = \Gamma \left(\tilde{T}_i + \tilde{T}_{ii} + \frac{1}{4} \sum_{j>i}^4 \tilde{T}_{ij} + \frac{1}{4} \sum_{h=1}^{i-1} \tilde{T}_{hi} \right) - \Xi \tilde{V}_{ii}, \tag{15a}$$

and

$$\frac{d\tilde{V}_{ij}}{d\tilde{t}} = \frac{1}{2} \Gamma \tilde{T}_{ij} - \Xi \tilde{V}_{ij}, i \neq j. \tag{15b}$$

We solve the dimensionless Equations 5 and 11–15 as follows. We recognize that the equations are strongly coupled because of the integral equation formalism (Equation 12) employed; for instance, evaluation of the integral in Equation 12a to determine $\tilde{T}_i(\tilde{t})$ requires knowledge of \tilde{V}_{jh} at all times from 0 to \tilde{t} , which in turn depends on \tilde{T}_i through Equation 15. Using the initial conditions, we first integrate the differential equations for \tilde{T} and \tilde{V}_{jh} (Equations 11 and 15) for a small time step θ , i.e., from $\tilde{t} = 0$ to $\tilde{t} = \theta$. Next, we integrate the differential equations for the conditional probabilities M (Equation 14) by discretizing $\tilde{\tau}$, which can vary from 0 to θ , into intervals of length θ_m and determining $\tilde{V}_{jh}(\alpha\theta_m)$, where α assumes integer values from 0 to $\theta\theta_m$, by linear interpolation between $\tilde{V}_{jh}(0)$ and $\tilde{V}_{jh}(\theta)$. We then evaluate the integrals in Equation 12 to determine $\tilde{T}_i(\theta)$, $\tilde{T}_{ii}(\theta)$, and $\tilde{T}_{ij}(\theta)$. We march forward in time and evaluate $\tilde{T}(2\theta)$ and $\tilde{V}_{jh}(2\theta)$ by integrating Equations 11 and 15 from time $\tilde{t} = \theta$ to $\tilde{t} = 2\theta$, integrate Equation 14 by allowing $\tilde{\tau}$ to vary from 0 to 2 θ , and evaluate the integrals in Equation 12 to determine $\tilde{T}_i(2\theta)$, $\tilde{T}_{ii}(2\theta)$, and $\tilde{T}_{ij}(2\theta)$. We repeat the procedure until $\tilde{t} = 10\delta$ (i.e., $t = 10$ d). The solution is implemented by a computer program written in Fortran 90.

Scaling analysis. We derive below the scaling relationships mentioned in Equation 7. Following the onset of infection, for times small compared to the timescale of CD4 down-modulation, i.e., $t \ll t_d$, because $k \approx k_0$, we write the dynamics of singly infected cells as

$$\frac{dT_1}{dt} = k_0 T \sum_{k=j}^4 \sum_{j=1}^4 R_1(jk) V_{jk}(t) - k_0 T_1 V - \delta T_1, \tag{16}$$

where the first term on the right-hand side is the rate of formation of T_1 by the infection of uninfected cells, and the second and third terms are the losses of T_1 due to further infections and cell death. At the start of infection, the dominant viral populations are V_{11} and V_{22} (Figure 3B), of which infection by the former alone yields T_1 . Further, because T_1 is small (Figure 3A), the loss terms, which are linear in T_1 , are negligible. Equation 16 then simplifies to

$$\frac{dT_1}{dt} \approx k_0 T V_{11}. \quad (17)$$

For lengths of time short compared to the timescales over which V and T change, we let $T \approx T_0$ and $V_{11} \approx V_0$ and integrate Equation 17 to obtain

$$T_1 \approx k_0 T_0 V_0 t, \quad (18)$$

where we use the initial condition $T_1(0) = 0$. With assumptions similar to those employed in obtaining Equation 17, we find that the coinfecting cell population evolves according to the following equation:

$$\frac{dT_{12}}{dt} \approx k_0 T_1 V_{22} + k_0 T_2 V_{11} = 2k_0 T_1 V_0, \quad (19)$$

where we recognize that $T_1 = T_2$ and $V_{11} = V_{22} \approx V_0$. Substituting for T_1 from Equation 18 and integrating with the initial condition $T_{12}(0) = 0$, we get

$$T_{12} \approx k_0^2 T_0 V_0^2 t^2. \quad (20)$$

The evolution of the heterozygous viral population, V_{12} , is given by

$$\frac{dV_{12}}{dt} \approx \frac{1}{2} N \delta T_{12},$$

where we note that 1/2 of the virions produced from cells T_{12} are heterozygous. We ignore viral clearance because V_{12} is expected to be small. Substituting for T_{12} from Equation 20 and integrating with the initial condition $V_{12}(0) = 0$, we obtain

$$V_{12} \approx \frac{1}{6} N \delta k_0^2 T_0 V_0^2 t^3. \quad (21)$$

The time evolution of the cell population infected with recombinants, T_4 , is then given by

$$\frac{dT_4}{dt} \approx k_0 T_0 V_{12} R_4(12), \quad (22)$$

where we recognize that because $V_{12} \gg V_{44} \gg V_{14}$, most of the cells T_4 are formed due to infection by V_{12} followed by recombination. Substituting for V_{12} from Equation 21, and integrating with the initial condition that $T_4(0) = 0$, we find

$$T_4 \approx \frac{1}{24} R_4(12) N \delta k_0^3 T_0^2 V_0^4 t^4. \quad (23)$$

Because the total infected cell population comprises largely cells T_1 and T_2 , which in turn are significantly smaller in number than uninfected cells (Figures 2 and 3A), we obtain the total percentage of infected cells,

$$p^* = \frac{100T^*}{T^* + T} \approx \frac{200T_1}{T_0} = 200k_0 V_0 t. \quad (24)$$

Similarly, the percentage of coinfecting cells,

$$p_{12} = \frac{100T_{12}}{T^* + T} \approx 100k_0^2 V_0^2 t^2, \quad (25)$$

and the percentage of cells infected with recombinants,

$$p_4 = \frac{100T_4}{T^* + T} \approx \frac{25}{6} R_4(12) N \delta k_0^3 T_0 V_0^4 t^4. \quad (26)$$

Combining Equations 24–26, we obtain

$$p_{12} \approx \frac{1}{400} (p^*)^2 \text{ and } p_4 \approx \frac{R_4(12) N \delta T_0}{2,400 k_0 V_0^2} (p_{12})^2. \quad (27)$$

We thus find that early during infection, the scaling laws $p_{12} \sim (p^*)^2$ and $p_4 \sim (p_{12})^2$ hold.

We next consider times longer than the timescale over which viral production and clearance reach pseudo steady state, $t > t_{\text{eq}}$. The magnitudes of the viral subpopulations still follow $V_{11} = V_{22} \gg V_{12} \gg V_{44}$ (Figure 3B). Similarly, for the infected cell subpopulations, we have $T_1 = T_2 \gg T_{12} \gg T_4$ (Figure 3A). The relevant evolution equations may then be written as

$$\frac{dT_1}{dt} \approx k_0 T V_{11} - k_1 T_1 V - \delta T_1, \quad (28)$$

$$\frac{dT_{12}}{dt} \approx k_1 T_2 V_{11} + k_1 T_1 V_{22} - \delta T_{12} \approx 2k_1 T_1 V_{11} - \delta T_{12}, \quad (29)$$

$$\frac{dT_4}{dt} \approx k_0 T V_{12} R_4(12) - \delta T_4, \quad (30)$$

$$\frac{dV_{11}}{dt} = N \delta T_1 - c V_{11}, \quad (31)$$

and

$$\frac{dV_{12}}{dt} = \frac{1}{2} N \delta T_{12} - c V_{12}, \quad (32)$$

where we let k_1 be the “mean” infection rate of singly infected cells. We note that k_1 is a function of the CD4 down-modulation timescale, t_d . If t_d is large, for instance, then $k_1 \approx k_0$. Applying the pseudo steady state approximation for the viral populations yields

$$V_{11} = \frac{N \delta T_1}{c} \text{ and } V_{12} = \frac{N \delta T_{12}}{2c}. \quad (33)$$

Substituting for V_{11} from Equation 33 in Equation 28, we obtain

$$\frac{dT_1}{dt} \approx k_0 T \frac{N \delta T_1}{c} - k_1 T_1 V - \delta T_1. \quad (34)$$

Assuming that changes in the target cell population, T , and the total viral load, V , occur slowly compared to changes in T_1 , which is expected in the initial stages of infection, we integrate Equation 34 to obtain

$$T_1 = T_1^{\text{eq}} \exp(Kt) \quad (35)$$

where $K = \frac{k_0 T N \delta}{c} - k_1 V - \delta$ and T_1^{eq} is the value of T_1 when $t = t_{\text{eq}}$. Note that in Equation 35, $t \gg t_{\text{eq}}$. Substituting for V_{11} and T_1 in Equation 29 yields

$$\frac{dT_{12}}{dt} \approx \frac{2k_1 N \delta}{c} (T_1^{\text{eq}})^2 \exp(2Kt) - \delta T_{12},$$

which upon integrating with the initial condition $T_{12} = T_{12}^{\text{eq}}$ when $t = t_{\text{eq}}$ and recognizing that $T_{12}^{\text{eq}} \ll T_1^{\text{eq}}$ gives

$$T_{12} = \frac{2k_1 N \delta}{c(2K + \delta)} (T_1^{\text{eq}})^2 \exp(2Kt) = \frac{2k_1 N \delta}{c(2K + \delta)} (T_1)^2. \quad (36)$$

Combining Equations 30, 33, and 36, we get

$$\frac{dT_4}{dt} \approx \left(\frac{N \delta}{c} \right)^2 \frac{k_1 k_0 T R_4(12)}{(2K + \delta)} (T_1^{\text{eq}})^2 \exp(2Kt) - \delta T_4. \quad (37)$$

Integrating Equation 37 and assuming $T_4 \ll T_{12}^{\text{eq}}$ yields

$$T_4 \approx \left(\frac{N \delta}{c} \right)^2 \frac{k_1 k_0 T R_4(12)}{(2K + \delta)^2} (T_1^{\text{eq}})^2 \exp(2Kt) = \frac{N \delta k_0 T R_4(12)}{2c(2K + \delta)} T_{12}. \quad (38)$$

Again, assuming that the singly infected cells are predominant in the infected cell population, the percentage of total infected cells is

$$p^* = \frac{100T^*}{T^* + T} \approx \frac{200T_1}{T}, \quad (39)$$

where the small percentage of infected cells allows us to write $T^* + T \approx T$. The percentage of coinfecting cells is then

$$p_{12} = \frac{100T_{12}}{T^* + T} \approx \frac{100}{T} \frac{2k_1 N \delta}{c(2K + \delta)} (T_1)^2 = \frac{1}{200} \frac{k_1 N \delta T}{c(2K + \delta)} (p^*)^2 \approx \frac{1}{400} \frac{k_1}{k_0} (p^*)^2, \quad (40)$$

where the last approximation follows from the sharp rise in T_1 following the establishment of pseudo steady state (Figure 3A), which according to Equation 34 implies that $K = \frac{k_0 T N \delta}{c} - k_1 V - \delta \approx \frac{k_0 T N \delta}{c}$. Finally, the percentage of cells T_4 infected with recombinants is

$$p_4 = \frac{100T_4}{T^* + T} \approx \frac{100 N \delta k_0 T R_4(12)}{2c(2K + \delta) T} T_{12} = \frac{R_4(12)}{4} p_{12}. \quad (41)$$

Thus, later in the infection ($t > t_{\text{eq}}$), the scaling laws $p_{12} \sim (p^*)^2$ and $p_4 \sim p_{12}$ hold.

Acknowledgments

Author contributions. NMD conceived and designed the experiments. GWS performed the experiments. GWS and NMD analyzed the data and contributed reagents/materials/analysis tools. NMD wrote the paper.

Funding. This work was supported by US National Institutes of Health grant AI065334.

Competing interests. The authors have declared that no competing interests exist.

References

- Blackard JT, Cohen DE, Mayer KH (2002) Human immunodeficiency virus superinfection and recombination: Current state of knowledge and potential clinical consequences. *Clin Infect Dis* 34: 1108–1114.
- Moutouh L, Corbeil J, Richman DD (1996) Recombination leads to the rapid emergence of HIV-1 dually resistant mutants under selective drug pressure. *Proc Natl Acad Sci U S A* 93: 6106–6111.
- Rhodes T, Wargo H, Hu WS (2003) High rates of human immunodeficiency virus type 1 recombination: Near-random segregation of markers one kilobase apart in one round of viral replication. *J Virol* 77: 11193–11200.
- Chen J, Dang Q, Unutmaz D, Pathak VK, Maldarelli F, et al. (2005) Mechanisms of nonrandom human immunodeficiency virus type 1 infection and double infection: Preference in virus entry is important but is not the sole factor. *J Virol* 79: 4140–4149.
- Dang Q, Chen JB, Unutmaz D, Coffin JM, Pathak VK, et al. (2004) Nonrandom HIV-1 infection and double infection via direct and cell-mediated pathways. *Proc Natl Acad Sci U S A* 101: 632–637.
- Jung A, Maier R, Vartanian JP, Bocharov G, Jung V, et al. (2002) Multiply infected spleen cells in HIV patients. *Nature* 418: 144.
- Levy DN, Aldrovandi GM, Kutsch O, Shaw GM (2004) Dynamics of HIV-1 recombination in its natural target cells. *Proc Natl Acad Sci U S A* 101: 4204–4209.
- Jetz AE, Yu H, Klarmann GJ, Ron Y, Preston BD, et al. (2000) High rate of recombination throughout the human immunodeficiency virus type 1 genome. *J Virol* 74: 1234–1240.
- Galletto R, Negroni M (2005) Mechanistic features of recombination in HIV. *AIDS Rev* 7: 92–102.
- Shriner D, Rodrigo AG, Nickle DC, Mullins JI (2004) Pervasive genomic recombination of HIV-1 in vivo. *Genetics* 167: 1573–1583.
- Charpentier C, Nora T, Tenaillon O, Clavel F, Hance AJ (2006) Extensive recombination among human immunodeficiency virus type 1 quasispecies makes an important contribution to viral diversity in individual patients. *J Virol* 80: 2472–2482.
- McCutchan FE (2006) Global epidemiology of HIV. *J Med Virol* 78: S7–S12.
- Chen J, Rhodes TD, Hu WS (2005) Comparison of the genetic recombination rates of human immunodeficiency virus type 1 in macrophages and T cells. *J Virol* 79: 9337–9340.
- Rhodes TD, Nikolaitchik O, Chen JB, Powell D, Hu WS (2005) Genetic recombination of human immunodeficiency virus type 1 in one round of viral replication: Effects of genetic distance, target cells, accessory genes, and lack of high negative interference in crossover events. *J Virol* 79: 1666–1677.
- Perelson AS (2002) Modelling viral and immune system dynamics. *Nat Rev Immunol* 2: 28–36.
- Nowak MA, May RM (2000) *Virus dynamics: Mathematical principles of immunology and virology*. New York: Oxford University Press.
- Simon V, Ho DD (2003) HIV-1 dynamics in vivo: Implications for therapy. *Nat Rev Microbiol* 1: 181–190.
- Althaus CL, Bonhoeffer S (2005) Stochastic interplay between mutation and recombination during the acquisition of drug resistance mutations in human immunodeficiency virus type 1. *J Virol* 79: 13572–13578.
- Bocharov G, Ford NJ, Edwards J, Breinig T, Wain-Hobson S, et al. (2005) A genetic-algorithm approach to simulating human immunodeficiency virus evolution reveals the strong impact of multiply infected cells and recombination. *J Gen Virol* 86: 3109–3118.
- Bretscher MT, Althaus CL, Muller V, Bonhoeffer S (2004) Recombination in HIV and the evolution of drug resistance: for better or for worse? *Bioessays* 26: 180–188.
- Carvajal-Rodriguez A, Crandall KA, Posada D (2007) Recombination favors the evolution of drug resistance in HIV-1 during antiretroviral therapy. *Infect Genet Evol* 7: 476–483.
- Fraser C (2005) HIV recombination: what is the impact on antiretroviral therapy? *J R Soc Interface* 2: 489–503.
- Rouzine IM, Coffin JM (2005) Evolution of human immunodeficiency virus under selection and weak recombination. *Genetics* 170: 7–18.
- Bonhoeffer S, Chappey C, Parkin NT, Whitcomb JM, Petropoulos CJ (2004) Evidence for positive epistasis in HIV-1. *Science* 306: 1547–1550.
- Kouyos RD, Althaus CL, Bonhoeffer S (2006) Stochastic or deterministic: what is the effective population size of HIV-1? *Trends Microbiol* 14: 507–511.
- Chen BK, Gandhi RT, Baltimore D (1996) CD4 down-modulation during infection of human T cells with human immunodeficiency virus type 1 involves independent activities of vpu, env, and nef. *J Virol* 70: 6044–6053.
- Lama J (2003) The physiological relevance of CD4 receptor down-modulation during HIV infection. *Curr HIV Res* 1: 167–184.
- Piguet V, Gu F, Foti M, Demareux N, Gruenberg J, et al. (1999) Nef-induced CD4 degradation: a diacidic-based motif in Nef functions as a lysosomal targeting signal through the binding of beta-COP in endosomes. *Cell* 97: 63–73.
- Dixit NM, Perelson AS (2005) HIV dynamics with multiple infections of target cells. *Proc Natl Acad Sci U S A* 102: 8198–8203.
- (2005) Correction for Levy et al. From the cover: dynamics of HIV-1 recombination in its natural target cells, *PNAS* 2004 101: 4204–4209. *Proc Natl Acad Sci U S A* 102: 1808.
- Speirs C, van Nimwegen E, Bolton D, Zavolan M, Duvall M, et al. (2005) Analysis of human immunodeficiency virus cytopathicity by using a new method for quantitating viral dynamics in cell culture. *J Virol* 79: 4025–4032.
- Dixit NM, Perelson AS (2004) Multiplicity of human immunodeficiency virus infections in lymphoid tissue. *J Virol* 78: 8942–8945.
- Sato H, Orenstein J, Dimitrov D, Martin M (1992) Cell-to-cell spread of HIV-1 occurs within minutes and may not involve the participation of virus-particles. *Virology* 186: 712–724.
- Mansky LM, Temin HM (1995) Lower in-vivo mutation-rate of human-immunodeficiency-virus type-1 than that predicted from the fidelity of purified reverse-transcriptase. *J Virol* 69: 5087–5094.
- Perelson AS, Neumann AU, Markowitz M, Leonard JM, Ho DD (1996) HIV-1 dynamics in vivo: virion clearance rate, infected cell life-span, and viral generation time. *Science* 271: 1582–1586.
- Ribeiro RM, Bonhoeffer S (2000) Production of resistant HIV mutants during antiretroviral therapy. *Proc Natl Acad Sci U S A* 97: 7681–7686.
- Clavel F, Hance AJ (2004) Medical progress: HIV drug resistance. *N Engl J Med* 350: 1023–1035.
- Kellam P, Larder BA (1995) Retroviral recombination can lead to linkage of reverse-transcriptase mutations that confer increased zidovudine resistance. *J Virol* 69: 669–674.